Evaporation over fresh and saline water using SEBS

AHMED RAGAB ABDELRADY
March, 2013

SUPERVISORS:
Dr. J. (Joris) Timmermans
Dr. Z. (Zoltan) Vekerdy

Evaporation over fresh and saline water using SEBS

AHMED RAGAB ABDELRADY

Enschede, The Netherlands, March, 2013

Thesis submitted to the Faculty of Geo-Information Science and Earth Observation of the University of Twente in partial fulfilment of the requirements for the degree of Master of Science in Geo-information Science and Earth Observation.
Specialization: Water resource and environmental management

SUPERVISORS:
Dr. Joris Timmermans
Dr. Zoltán Vekerdy

THESIS ASSESSMENT BOARD:
Prof.dr. ing. W. (Wouter) Verhoef (Chairman)
Prof.Dr. Li Jia (External Examiner, Alterra Univeristeit Wageningen)

ABSTRACT

Evaporation over large water bodies has a crucial role in the global hydrological cycle. Evaporation occurs whenever there is a vapour pressure deficit between a water surface and the atmosphere. In addition the available energy needs to be sufficient for vaporization (to enable a phase change from liquid to gaseous state). Different models have been developed to estimate the evaporation process over water surfaces using earth observation data. Most of these models are concerned with the atmospheric parameters. However, these models do not take into account the influence of salinity on the evaporation rate. Water salinity affects both the density and latent heat of vaporization of the water body and as a consequence reflects on the evaporation rate. The current models do not consider the difference in the energy needed for vaporization. For this purpose, an energy balance model is required.

Several energy balance models, such as the surface energy balance system (SEBS), that calculate daily evapotranspiration exist, They estimate the heat fluxes by integration of satellite data and hydro-meteorological field data. SEBS has the advantage that it can be applied over a large scale because it incorporates the physical state of the surface and the aerodynamic resistances in the daily evapotranspiration estimation. Nevertheless, this model has not used over water surfaces.

The goal of this research is to adapt SEBS to estimate the daily evaporation over fresh and saline water bodies. In particular, 1) parameterizations required for water heat flux and sensible heat flux (through the roughness heights for momentum and heat transfer) need to be updated, 2) upscaling to daily evaporation needs to be investigated and finally, 3) integration of the salinity factor to estimate the evaporation over saline water needs to be performed.

Eddy covariance measurements over the Ijsselmeer Lake (The Netherlands) was used to estimate the roughness heights for momentum and heat transfer at respectively 0.0002 and 0.0001 m. Application of these values over Victoria and Tana Lakes (freshwater), in Africa showed latent heat to be in a good agreement with the measurements, with RMSE of 19.7 and 35.5 [W m^{-2}] and rRMSE of 4.1% and 4.7 %, respectively. Afterwards, the validity of salinity adapted model was tested over different study areas using ECMWF data. It was found that for the original SEBS model and salinity-adapted model over Great Salt Lake, the RMSE are 0.62 and 0.24 [mm $3h^{-1}$], respectively and the rRMSE 19% and 24%. The evaporation reduction of the Great Salt Lake and the oceans are 27% and 1 %, respectively. In conclusion, SEBS model is adapted to calculate the daily evaporation over fresh water and salt water by integration the salinity factor in the model.

ACKNOWLEDGEMENTS

Alhamedlleiha, praise to be Allah, I cannot achieve anything without his will, permission and supporting. All the knowing and the powerful for supporting me to get my first step in the excellent world of science.

I would like to provide my gratitude to the Citadel foundation for granting me this opportunity to pursue my Master of Science degree in water science.

I would like to provide my sincere gratitude to Dr. Joris Timmermans, my first supervisor, for his excellent guidance and encouragement during the research period. He is almost opened up to me with enormous knowledge and continuous advices. I am also deeply thankful to Dr. Zoltan Vekerdy, my second supervisor for being supportive and provided me with valuable comments which help me a lot to improve the quality of my thesis.

I am greatly indebted to Dr. M.S. Salama for his continuous support and advice during my master studying. I am also thankful to Dr. Christiaan van der Tol for providing data about Lake Tana. I am also thankful to Ing. Murat Ucer for his supporting and helping during the fieldwork period.
I would like to acknowledge ECMWF for providing freely accessible data for my work.

I would like to thank all the WREM staff members at ITC. They almost there helping me and enriching my acknowledgement. Special thanks to my classmates for their friendship and co-operation during the period of study.

Last but not the least, my deepest gratitude goes to my parents, brother and sisters. I cannot be here without their supporting and encouragement during my life.

TABLE OF CONTENTS

LIST OF FIGURES

LIST OF TABLES

LIST OF ACRONYMS

AATSR	Advanced Along-Track Scanning Radiometer
ASL	Atmospheric Surface layer
BAS	Bulk Atmospheric Similarity
ECMWF	European Centre for Medium range Weather Forecasts
ESA	European Space Agency
ETM	Equilibrium Temperature Model
MOS	Monin-Obukhov Similarity
RMSR	Root Mean Square Error
rRMSE	relative Root Mean Square Error
SEBS	Surface Energy Balance System
STD	Standard Deviation

1. INTRODUCTION

1.1. Background

"Salinity is the ocean signature of the global water cycle" (Schmitt et al., 1995). Salinity is one of the most important parameters among the water quality parameters that affect the hydrological cycle and the interaction between the water surface and the atmosphere. It has a great effect on the exchange of gases through the air-water interface. Salinity has a significant influence upon the surface specific humidity gradient as it decreases the surface vapour pressure; thus it affects the evaporation rate (Font et al., 2010). However, current atmospheric circulation models used in climatic studies still ignore its influence upon evaporation. An example of the importance of salinity and its influence on the global climate and water cycle is the "great salinity anomaly". In 1970, a large amount of less saline and low temperature water from the Arctic flowed into the northerly part of the North Atlantic via the Fram Strait. It largely decreased the temperature of air in the northern Europe and influenced on the energy balance system and the evaporation rate on this region (Belkin et al., 1998; Dickson et al., 1988).

Salinity influences on the physical properties of water such as density, latent heat of vaporization and boiling point. The density gradient plays an important role in the horizontal circulation and thermohaline circulation of the ocean, and thus it has an effect on the convectional water depth. Moreover, it forces the ocean currents that able to transfer a large amount of heat around the world, and modulate the global climate (Le Vine et al., 2010). From another point of view, an increase in the salinity results in increasing the boiling point of the water. Therefore the surface vapour pressure will decrease (Al-Shammiri, 2002). In the same regard, salinity has a great influence on the latent heat of vaporization. That is the amount of heat energy required to change the water state from liquid to vapour state. It also can be defined as the difference between the fresh water vapour's specific enthalpy and partial specific enthalpy of sea water. Based on this definition, many models were developed to estimate the latent heat of vaporization as a function of latent heat of vaporization of fresh water multiply by a salinity factor (Bromley et al., 1974; Sharqawy et al., 2011).

The extent of salinity contribution to the reduction of evaporation from a large water body depends on the water composition. Types of salt in the water define the evaporation reduction percentage. If the atmospheric humidity is above 70% and the water body is saturated with Sodium chloride, there will be no evaporation. In the same regard, if the water body is saturated with magnesium chloride, no evaporation will happen at lower relative humidity percentage (Leaney, 2000). It was investigated by (Turk, 1970) that the increase of salinity from zero to 200 [g l^{-1}] will lead to decrease the rate of evaporation by 10%. For increasing the salinity to 320 [g l^{-1}], the evaporation rate will decrease about 20%, according to experiments made above a water pan.

Evaporation over a water body has an influential role in the hydrological cycle, as it is the common parameter in the energy and water balance equations. Knowing the amount of water evaporated from any water body into the atmosphere is a crucial step in different aspects of the management of water resources

for different purposes such as wetlands' management, design of water storage reservoirs, and surface water system studies (Finch, 2001; Hudlow et al., 1983; Marsh et al., 1988; Mengistu et al., 2010) .

1.2. Sociological problems

During the last decades, as a result of high evaporation and low recharge, severe water quality problems related to salinity have occurred in many lakes in different climatic regions around the world such as the Qaroun Lake in Egypt. Increased salinity resulted in change of the lake's hydrological cycle and destroying the aquatic life of these lakes. Qaroun Lake has a very high economic importance in Egypt. It is the main water resource of irrigation in the fayoum basin. It is also a valuable source of fish. Moreover, it is a natural reserve so it is attractive place for tourism.

The characteristics of the lake have changed considerably in the last decades due to the high evaporation rate and low recharge. The lake now is mainly fed by agricultural drainage water mixed with effluents from municipalities and industries with high concentration of salinity. The area of the lake declines quickly. This decrease in lake level is parallel followed by an increase in salinity. As a result the economic benefits of the lake decline swiftly, and the aquatic environment has been destroyed. Many studies were developed to estimate the evaporation rate and control the salinity in the lake (Ali, Madramootoo, & Abdel-Dayem, 2000), (Ali, Madramootoo, Abdel-Dayem, et al., 2000), (Ali et al., 2001). Therefore, knowing the relationship between salinity and evaporation and how it can affect other energy balance terms is very important in the modelling and management of such a saline lake system.

1.3. Problem statement

It is hard to estimate evaporation over water accurately based on meteorological parameters' measurements over the water surface. Evaporation over water surfaces depend on the atmospheric conditions, but it is largely controlled by the surface water state and the water composition. Different methods had been developed in the last few decades to estimate the rate of evaporation over water bodies. These methods are based on the remote-sensing techniques, physical models or both (Tanny et al., 2008). More than 30 equations have been developed to estimate the evaporation (Winter et al., 1995), but most of them did not consider the effect of water composition on the evaporation rate.

In contrast, many studies have been developed to estimate the influence of salinity upon the evaporation process. However, Most of them were done inside the laboratories with special apparatus and under controlled conditions for industrial purposes (Al-Shammiri, 2002) and (Oroud, 1999). (Schuepp et al., 1990) and (Salhotra et al., 1987) developed a model to estimate the influence of salinity on the shallow lake evaporation, but it did not account for the energy balance terms. This model uses the ratio between saline water evaporation and hypothetical freshwater evaporation term.

Monitoring of evaporation with remote sensing requires a fine-tuning of evaporation rates from open water bodies. The water composition and the physical state of the surface should be considered, this would lead to a more accurate water balance calculations. It was investigated by (Harbeck, 1955) and (Turk, 1970) that the influence of salinity variations in the water density, and the evaporation rate is more important than other water quality parameters. Therefore, this study focuses on getting a surface energy

balance model based on remote sensing data to estimate the evaporation rate over fresh and saline water surfaces.

1.4. Objectives and questions

The major objective of this research is to integrate satellite data and in-situ data to estimate the evaporation rate over fresh and saline water bodies. Evaporation cannot be estimated directly from satellite imagery; instead, the surface energy balance has to be calculated to derive evaporation. Several models have been developed to estimate evapotranspiration, like the SEBS model.

The SEBS algorithm was developed by (Su, 2002b) to estimate the heat fluxes by integration of satellite data and hydro-meteorological field data. It's one source physical model applicable on a large scale, as it incorporates the physical state of the surface and the aerodynamic resistances for the daily evaporation estimation. It has been validated in several studies on the land, but hardly any researcher has applied it on water bodies. Therefore the main goal can be split up into the specific objectives:

a. Adapt the energy balance part of SEBS model to fresh water.
    1. Develop and validate a model to estimate the water heat flux.
    2. Estimate the roughness heights for momentum and heat transfer.
    3. Validate the adapted SEBS model over fresh water bodies
b. Adapt the evaporation part of SEBS model to saline water.
    1. Estimate the sensitivity of the latent heat of vaporization to the salinity change.
    2. Analyses and estimate the influence of salinity upon evaporation of a large water body.
    3. Validate the adapted salinity – SEBS model over different water bodies with different salinities.

In order to achieve these objectives, the following questions should be addressed:

- How large is the contribution of the water heat flux to the surface energy balance?
- What are the roughness heights for momentum and heat transfer of water?
- What is the accuracy of the latent heat flux and daily evaporation estimations over fresh water using the SEBS model?
- How much does the evaporation rate change with water salinity variations?
- What is the uncertainty of the new algorithm in estimating evaporation over saline water surfaces?
- To which extent can the salinity reduce the evaporation over hyper-saline water body?

1.5. Assumption

In order to achieve the main objective, the physical water characteristics should not be affected largely by the other quality parameters, therefore the following assumption is made:

- The evaporation rate is not affected significantly by the suspended matters or coloured dissolved materials in the water.
- The energy balance terms are not significantly affected by salinity. Therefore we are allowed to use fresh water parameterizations over salt lakes. The assumption is that only the latent heat of vaporization is changed.

2. METHODOLOGY

A method is applied in this research is illustrated in (Figure 2-1).

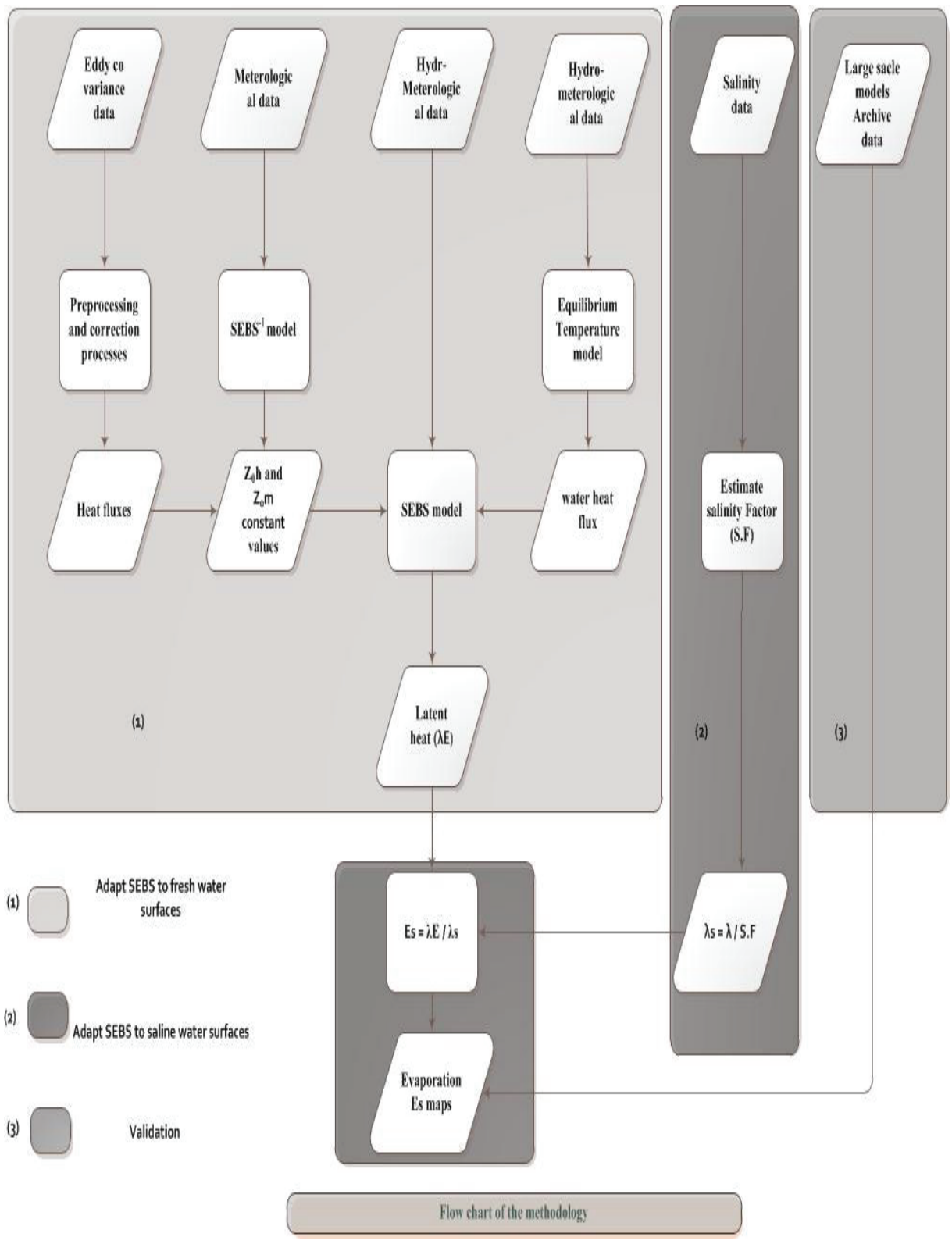

Figure 2-1. Methodology flow chart

In order to estimate evaporation over water using remote sensing, adaptation of the SEBS model (Su et al., 2001) is required. This is done in three steps: first the energy balance part needs to be adapted for water, secondly the salinity part must be implemented and finally the adaptions need to be evaluated.

1. Within the adaptation of the SEBS model it is assumed that salinity has only a minor influence on the energy balance. Therefore the modification of the energy balance part is the same for fresh and salt water. In that case three parameters are of vital importance: the water heat flux, the roughness of heat transfer (Z_{oh}), and the roughness of momentum transfer (Z_{om}).

    a. The thermal equilibrium exchange model (Abualnaja, 2009) was incorporated to SEBS model to estimate the water heat flux. The input parameters include water surface temperature, dew temperature, wind speed and the net solar radiation.

    b. In this research, field measurements were performed over the Ijsselmeer. This data is used to estimate the (Z_{oh}) and (Z_{om}). First of all, The AltEddy and EddyPro tools were used to apply the correction processes on the eddy covariance data and to estimate the heat fluxes. The roughness height for heat transfer (Z_{oh}) was derived by inverse the sensible heat flux equation of SEBS model using (S. Liu et al., 2007) equations. The roughness height for momentum transfer (Z_{om}) was determined using (Tanny et al., 2008) model.

    c. These parameters are critical in implementation SEBS model for other study areas to estimate the heat fluxes. SEBS model (Su, 2002b) integrates between the hydro-meteorological, satellite and radiative forcing data on the other study areas to estimate the heat fluxes and the daily evaporation.

2. The salinity has a notable influence on the water physical properties; therefore, it affects the evaporation rate. The salinity factor was integrated with adapted SEBS to estimate the rate of evaporation over saline water surfaces.

3. Finally, the new approach has to be validated to provide more accurate evaporation maps for different water salinity concentrations. Therefore this adapted SEBS model was applied on various water bodies with diverse salinity concentrations, including fresh, saline and hypersaline water bodies. The outputs of the adapted SEBS model were compared with Bowen model (over Lake Tana) and ECMWF data for the rest study areas.

Part 1 represents the adaption of SEBS model for freshwater will be explained in more detail in paragraph 2.2; part 2 describes estimation the influence of salinity on the daily evaporation value will be explained in more detail in paragraphs 2.3; and part 3 involves the validation of the method will be described in more detail in paragraph 2.4.

2.1. SEBS Algorithm

SEBS (Su, 2002a) integrates satellite data and hydro-meteorological data to solve the energy balance (Equation 1) and to estimate the daily evaporation rate. SEBS requires three sets of data as input. Firstly, remote-sensing data includes (emissivity, surface albedo and water surface temperature). The second set is

the meteorological data set containing air pressure, temperature of air, relative humidity and wind speed at reference height. Thirdly, the radiative forcing parameters such as downward shortwave and longwave radiations are required. All the parameters should refer to the same time.
The energy budget model can express as:

$$R_n = G_0 - H - \lambda E \qquad \text{Equation 1}$$

Net radiation (R_n) in [W m^{-2}] is estimated as the sum of the net shortwave and longwave radiations. Water heat flux (G_0) in [W m^{-2}] is calculated by integration of the change of temperature with time at different depths or by using the equilibrium temperature model. The sensible heat flux (H) in [W m^{-2}] is estimated by iteration non-linear similarity equations. Finally, latent heat (λE) in [W m^{-2}] is calculated based on the energy balance theory at limiting cases.

2.1.1. Net radiation

The net radiation, i.e. the balance of the radiation at the surface of the water body influences the air temperature, the water heat content, and the water surface temperature. In addition, this parameter controls the turbulent fluxes at the water surfaces. The net radiation is estimated as the balance of the incoming and outgoing radiations.

2.1.2. Sensible heat

The sensible heat flux is a primary component of the SEBS algorithm. It expresses as the exchange of heat between the atmosphere and the surface through air molecules as a result of a vertical temperature gradient between the water surface and the atmosphere. The sensible heat is not only dependent on the surface state but also on the state of the atmosphere. Therefore, non-linear equations of Monin-Obukhov Similarity (MOS) are used to estimate the sensible heat flux, wind speed friction and the Monin-Obukhov height. The equations given by (Brutsaert, 1999) can be applied if the reference height above the water surface is few meters, where the surface heat fluxes are related to the atmosphere and surface variables.

2.1.3. Latent heat

Latent heat is estimated in SEBS using the evaporative fraction term. This can be calculated using the actual sensible heat. The actual sensible heat flux value is constrained between dry and wet sensible heat flux values. The dry sensible heat equals the difference between the net radiation and the water heat flux, whereas the latent heat flux equals zero. On contrast of dry conditions, the sensible heat flux will be the minimum, and evaporation will occur under wet conditions, i.e. at the potential rate.

2.1.4. Daily evaporation

Evaporation responds to the variations in the available energy in a diurnal way. Therefore, the measurements of the evaporation should be continuously during the day. This is impractical for orbiting satellites. Remote sensing images of such satellites can be used to provide evaporation maps with high spatial resolution during overpass, but they are temporarily limited at a definite time during the day. A daily stable term as the evaporative fraction can be used with the satellite images to upscale the latent heat

and the evaporation rate from instantaneous to daily estimation. Evaporative fraction is the ratio between the latent heat and the available energy at the water surface. The stability of the evaporative fraction term was investigated by (Shuttleworth et al., 1989), (Nichols et al., 1993) and (Cragoa et al., 1996).

SEBS model estimates the daily evaporation rate based on the evaporative fraction term and the daily available energy. Over land, the daily ground heat flux was investigated to be zero. However, in this research, it is investigated that this character is not valid over water surfaces. Therefore, this part of SEBS model has to update.

2.2. Adaption SEBS to fresh water

SEBS model was adapted to estimate the daily evaporation rate over water surfaces (Figure 2-2). The most critical parameters in the SEBS model are water heat flux and the roughness heights for momentum and heat transfer (Z_{om} and Z_{oh})(Su, 2002a).

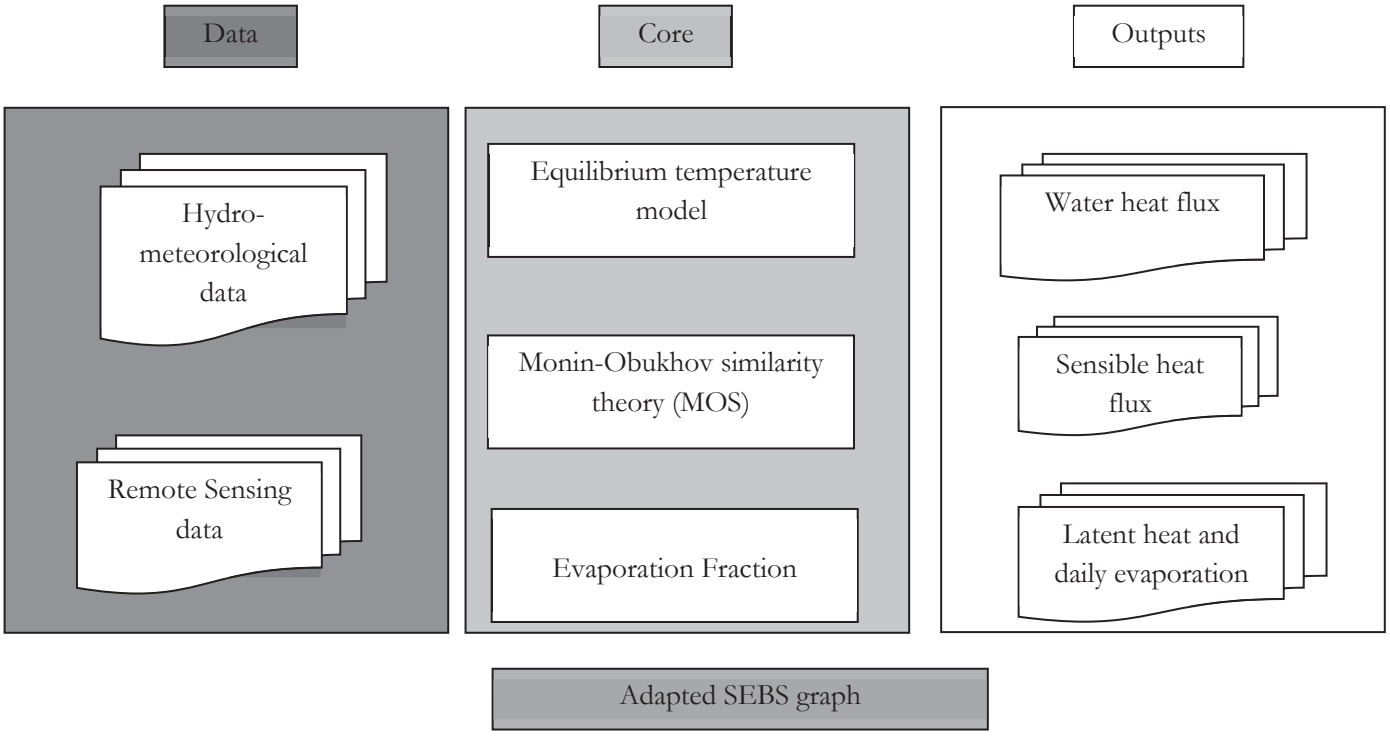

Figure 2-2.SEBS - Adapted Model graph

2.2.1. Water heat flux

Water heat flux (G_0) is the major component of the energy balance over water surfaces. It represents the change rate of the temperature with respect to depth and time. In other words, it is defined as the energy used to heat the water. The water heat flux (G_0) has two major components, the water heat storage (Q_t) (the rate of water heat content change) and the water transported through the water flow and other processes (Q_v) (Equation 2).

$$G_0 = Q_t + Q_v \quad \text{Equation 2}$$

It is positive when the water surface temperature is higher than the air temperature. Many studies neglect the value of water heat flux on a daily basis, as the energy gained during a daytime is lost in the night. However, it is investigated that this theory is not almost valid, but it depends on the surrounded atmospheric conditions and the amount of heat transported through the water flow. Moreover, it is still very important to estimate the periodic change of water temperature, as it is the main component of the energy balance equation affected by the water composition.

It has shown that the soil heat flux can be estimated using the surface temperature retrieved from remote-sensing data (Murray et al., 2007). However, there are some differences between soil and water heat fluxes, including:

- The heat energy transfer through the water body in a convectional and conduction ways.
- Water has different thermal characteristics than soil such as the stability of latent and sensible heat during the day.
- The water is mixed by the turbulent flux and eddy movement.
- The water surface features with transmittance and scattering characters.

Therefore, update the SEBS model with other appropriate water heat flux model is the main key of adaption SEBS model for estimation water bodies' evaporation. During this research, many methods tried out to have a good estimation of water heat flux according to the availability of the data.

2.2.1.1. Water temperature profile method

The water heat flux can be estimated using the mathematical Equation (3).

$$G_0 = \rho_w c_p \int_{z=0}^{z} \frac{\Delta T}{\Delta t} \Delta z \quad \text{Equation 3}$$

$\frac{\Delta T}{\Delta t}$	:	the change in temperature between two consecutive measurements	[m s^{-1}]
Δz	:	the thickness of water layer between two consecutive measurements	[m]
ρ_w	:	water density	[kg m^{-3}]
C_p	:	specific heat of air at constant pressure	[J kg^{-1} k^{-1}]

The difficulties of the field measurements on water surfaces limited the usage of this method. A new parameterization was originally planned using field data. However during the field work, the data of water temperature vertical profile had been lost. Instead other methods are investigated to estimate the water heat flux. During this research, different methods had been tried out to have a good estimation of water heat flux.

- Firstly, a threshold of 300 [W m^{-2}] of the net radiation selected to get a constant ratio between water heat flux and net radiation, when the net radiation is the main dominate factor on water heat flux. It is found that this ratio value changes regularly in a spatial and temporal way.

- After that, an equation relates the atmospheric parameters such as wind speed, temperature gradient as well as pressure deficit, and water heat flux had been created, as these parameters play a main role in the variations of the other heat fluxes terms, which directly affects the water heat flux. Nevertheless, it is proved that the equation's parameters change also continuously in a spatial and temporal way.
- Then, the inverse of penman equation has been tested. It is provided good results under high net radiation. However, a large error is obtained under low net radiation values.
- These methods provided approximately good results; however, a small error in the water heat flux estimation can lead to a high deviation in the latent heat estimation value than the true value, as water heat flux is the major heat fluxes component, and most of the water heat energy is retained in that term.
- Ultimately, the equilibrium temperature model developed by (Ahmad F et al., 1994) was used.

2.2.1.2. Equilibrium Temperature Model (ETM)

Water heat flux can be described as the imbalance between the solar radiation, thermal radiation, sensible heat and latent heat fluxes. The equilibrium temperature (T_e) is a hypothetical water surface temperature suggested by (Edinger et al., 1968). It represents the temperature at which the net heat fluxes exchanges between the water surface and the atmosphere equals zero theoretically. The thermal exchange coefficient (β) shows how the water surface temperature responds to the variations in the sensible, latent heat fluxes and the thermal radiations (Haney, 1971). The ETM model of (Ahmad F & Sar, 1994) integrates between the water surface temperature and the equilibrium temperature using the thermal exchange coefficient to estimate the water heat flux value (Figure 2-3). it can be shown that the water heat flux takes a negative value when the equilibrium temperature has lower value than the water surface temperature (Equation 4). In order to estimate the equilibrium temperature and the thermal exchange coefficient, as well as to derive the water heat flux, the following Equations (4, 5, 6, 7, 8, and 9) should be applied:

$$G_0 = \beta\,(T_e - \mathrm{T_0}) \qquad \text{Equation 4}$$

$$T_e = T_d + \frac{Q_s}{\beta} \qquad \text{Equation 5}$$

$$\beta = 4.5 + 0.05\,\mathrm{T_0} + (\eta + 0.47)\,\mathrm{S(W)} \qquad \text{Equation 6}$$

$$S(W) = 3.3\,u \qquad \text{Equation 7}$$

$$\eta = 0.35 + 0.015\,\mathrm{T_0} + 0.0012\,(\mathrm{T_n})^2 \qquad \text{Equation 8}$$

$$T_n = 0.5\,(T_0 - T_d) \qquad \text{Equation 9}$$

Where

T_e	:	equilibrium temperature	[°C]
T_d	:	dew temperature	[°C]
Q_s	:	net shortwave radiations	[W m^{-2}]
β	:	thermal exchange coefficient	[W m^{-2} °c^{-1}]
$S(W)$	:	wind function	[m s^{-1}]

This method had been applied in the some previous studies, e.g., (Ahmad F & Sar, 1994) and (Abualnaja, 2009) on monthly and seasonally basis. In this research, this method was applied to estimate the instantaneous water heat energy flux.

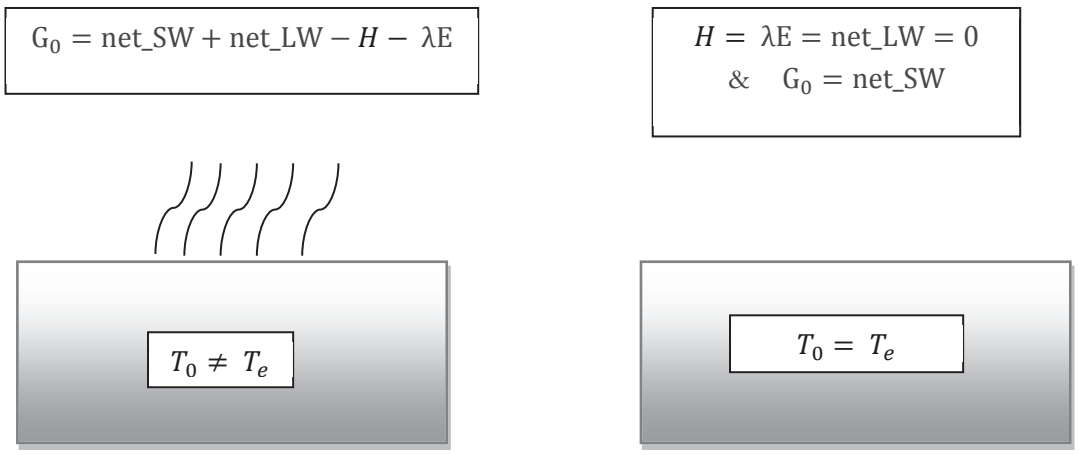

Figure 2-3.Equilibrium temperature model graph

net_SW is the net solar radiation
net_LW is the net thermal radiation

2.2.2. Sensible heat

Sensible heat describes as the aerodynamic resistance driven by the gradient temperature. Aerodynamic roughness height is a distinctive parameter in the sensible heat flux using a remote sensing tool. It has a great influence on the heat turbulent fluxes near the surface and the interaction between the water surface and the atmosphere. It is the main motivation factor of the forced convectional process over the surface. The roughness height for momentum and its counterpart for heat transfer are needed to estimate precisely, in order to have a good estimation of the aerodynamic resistance (van der Tol et al., 2012).

2.2.2.1. Roughness of momentum transfer (Z_{om})

The roughness height for momentum transfer (Z_{om}) and the zero displacement height (d_0) play a vital role in the Monin-Obukhov similarity theory (MOS) and the convectional heat transfer models. These two parameters significantly influence the momentum transfer between the water surface and the atmosphere (Koloskov et al., 2007). Z_{om} is the height that the momentum transfer is affected by surface characteristics (Jia et al., 2009b).

Despite this parameter is related to wind speed, atmospheric stratification and other factors; it can be considered as a constant value over a bluff-roughness surface like water bodies (Zhou et al., 2012).

Although it is difficult to get an accurate estimation of Z_{om}, many methods have been developed to get an exact estimation based on experimental measurements or remote-sensing techniques (Tian et al., 2011). In this research, the zero displacement height (d_0) is considered zero (Hudlow et al., 1983). (Tanny et al., 2008) model used to estimate the roughness for momentum during this study (Equation 10).

$$Z_{om} = \frac{u_*^2}{81\,g} \qquad \text{Equation 10}$$

Where

u^*	:	friction velocity	[m s^{-1}]
g	:	gravitational acceleration = 9.80665	[m s^2]

2.2.2.2. Roughness of heat transfer (Z_{oh})

The roughness height for heat transfer (Z_{oh}) is a crucial parameter in SEBS. It has a prominent effect on the heat transfer between the water surface and the atmosphere in terms of sensible heat flux. It is considered a critical parameter in the Monin-Obukhov similarity theory (MOS) which relates the surface fluxes to surface variables and variables in the atmospheric boundary-layer similarity (ASL), as well as in the bulk atmospheric boundary-layer similarity (BAS) which relates surface fluxes to surface variables and the mixed layer atmospheric variables (Brutsaert, 1999). Many studies have been developed to estimate Z_{oh} on land (Su et al., 2001), However, hardly any researcher determined it on a water surface. In this research, Z_{oh} was determined using eddy co variance heat fluxes and hydro-meteorological data by inverse the similarity equations of SEBS model. The roughness height for heat transfer also can be considered as a constant value over the bluff – rough surfaces (Cahill et al., 1997). The model of (S. M. Liu et al., 2007) was used to estimate the roughness of heat transfer on water surface (Equations 11,12).

$$KB^{-1} = \rho_a c_p \frac{(T_0 - T_a)}{H} ku^* - \ln\left(\frac{z-d_0}{z_{0m}}\right) + \varphi_h\left(\frac{Z-d_0}{L}\right) \qquad \text{Equation 11}$$

$$Z_{oh} = \frac{KB^{-1}}{Z_{om}} \qquad \text{Equation 12}$$

Where

k	:	Von Karman's constant = 0.4	[-]
B	:	Stanton number	[-]
T_0	:	surface temperature	[K]
T_a	:	air temperature	[K]
ρ_a	:	air density	[kg m^{-3}]
C_p	:	specific heat of air at constant pressure	[J kg^{-1} k^{-1}]

2.2.3. Daily evaporation

SEBS model estimates the daily evaporation rate based on the evaporative fraction term and the daily available energy. Evaporative fraction is calculated using the sensible heat values at dry and wet boundary conditions. The dry condition over water surfaces is considered when the water body is saturated with salt, and the relative humidity is higher than 70%. On the other hand, the lowest value of sensible heat is obtained under very low values of relative humidity. (Leaney, 2000) stated that if the relative humidity is higher than 70%, and the water body is saturated with sodium chloride; no evaporation will take place over the water surface. In the same regard, if the water body is saturated with magnesium chloride, no evaporation will occur at a lower limit of relative humidity. Hence, the evaporation process is bounded based on the water composition and the atmospheric conditions above the water surface (Figure 2-4)

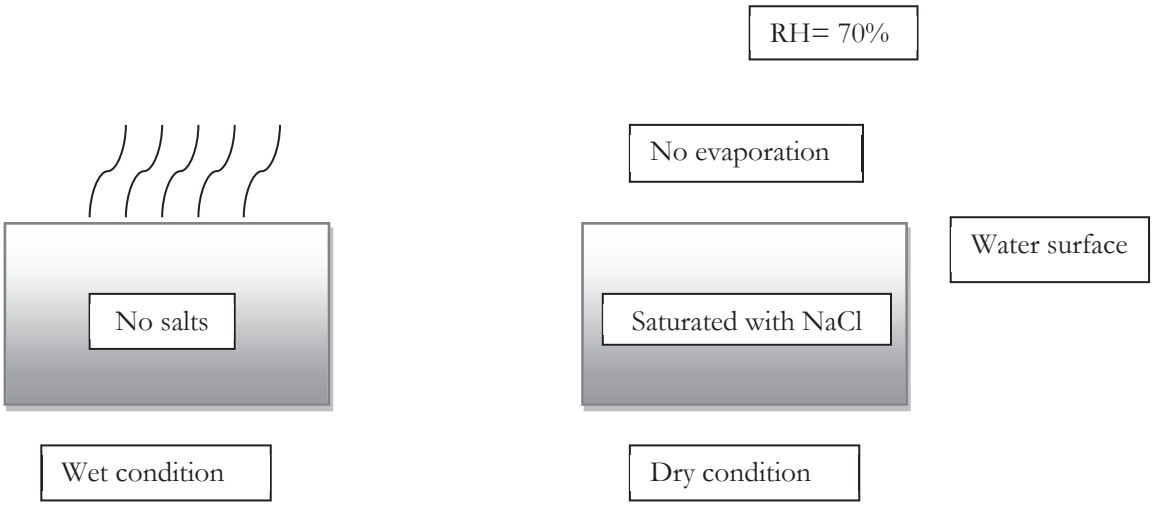

Figure 2-4.Dry and wet limits over water graph

According to (Manrique Suñén et al., 2012), latent and sensible heat follow a steady behaviour during the day. Therefore, the evaporative fraction is stable during the day; this character was investigated during this research. In the same regard, the available energy should also be stable during the day. This character of water bodies was also investigated during this research. From this point of view, the SEBS model is still valid to upscale the evaporation to a daily basis over water surfaces. The evaporative fraction integrates with the available energy to estimate the daily latent heat.

2.3. Adaption SEBS to saline water

The evaporation rate over a saline water surface is less than over fresh water under the same atmospheric conditions. The salinity influences on the latent heat of vaporization. Therefore it reduces the vapour pressure on the water surface, which directly influence on the evaporation rate. The influence of salinity on the latent heat of vaporization and evaporation rate can be expressed as a salinity factor. It represents the ratio of evaporation over saline water to fresh water in the identical atmospheric conditions. The salinity factor equation was deduced by (Turk, 1970) based on laboratory experiments (Equation 13).

$$\propto = 1.025 - 0.0246\, e^{0.00879\, S} \qquad \text{Equation 13}$$

$\propto$: Salinity reducing factor of evaporation

S : Salinity [g l^{-1}]

In this research, this equation was integrated with SEBS model to estimate the daily evaporation rate over saline water bodies.

2.4. Validation the adapted model

The adapted model had been validated on different spatial scales over different study areas with various salinity concentrations. Various statistical were used to assess the efficiency of the model on the evaporation rate estimation such as average, standard deviation (STD), Root Mean Square Error (RMSE) (Equation 14) and relative Root Mean Square Error (rRMSE) (Equation 15).

$$RMSE = \sqrt{\frac{\sum_{i=1}^{n}\left(X_i - \overline{X_i}\right)^2}{n}} \quad \text{Equation 14}$$

$$rRMSE = \left(\frac{RMSE}{\overline{X_{i_{max}}} - \overline{X_{i_{min}}}}\right) * 100 \quad \text{Equation 15}$$

X_i : model estimated parameter

$\overline{X_i}$: observation or ECMWF value

$\overline{X_{i_{max}}}$ and $\overline{X_{i_{min}}}$: maximum and minimum observation or ECMWF value

The estimated latent heat over Lake Tana was compared with the outputs of Bowen model. On the other hand, the results of daily evaporation rate over the other study areas were compared with ECMWF data to avoid the error produced as a result of uncertainty on the input atmospheric parameters.

2.5. Error analysis

The main objective of this process is to know to which extent each input parameter uncertainty can contribute to the error in the heat fluxes estimation using SEBS-adapted model. The sensitivity is estimated using direct and linear models. The direct model using the following (Equation 16):

$$S_i(Z_{\pm}) = \left(\frac{Z_{\pm} - Z_0}{Z_0}\right) * 100 \quad \% \quad \text{Equation 16}$$

S_i is the sensitivity function, Z_o, Z_+,Z_- are the estimated parameter when the input parameter equals reference, plus increment and minus increment, respectively.

The analytical linear method uses the first derivative of the estimated parameter relative to specific input parameter to estimate the sensitivity of the method as following (Equation 17):

$$S_i(P) = \frac{1}{Z}\left(\frac{\partial Z}{\partial P_i}\,\Delta P_i\right) * 100 \ \% \quad \text{Equation 17}$$

Z is the estimated parameter, P_i is the input parameter and ΔP_i is the increment value.

3. STUDY AREAS

The Ijsselmeer (the Netherlands) field work data was used to estimate the critical parameters of SEBS, including the roughness heights for momentum and heat transfer (Z_{om} and Z_{oh}). Then, the adapted SEBS model for freshwater was validated over the freshwater lakes Tana (Ethiopia) and Victoria (East Africa). After that, the adapted Salinity–SEBS model was used to estimate the turbulent heat fluxes and the daily evaporation from large water surfaces with different salinity levels such as the North Sea, Mediterranean Sea, Red Sea, Atlantic Ocean and Indian Ocean as well as the Great Salt Lake (USA).

3.1. IJsselmeer Lake

IJsselmeer is the largest lake in the Western Europe (Figure 3-1). This artificial lake covers about 1125 km^2 in the northern part of the Netherlands. The Ijsselmeer Lake was created in 1932 by the separation of the former Zuiderzee estuary from the North Sea by dam construction. Due to the land reclamation, the area of the lake was reduced rapidly. In 1975, the Houtribdijk dam was constructed to divide Ijsselmeer into two lakes: the Ijsselmeer Lake in the north and the Markermeer (ca. 650 km^2) in the south of the newly formed dam. Now it is considered a multifunctional area with various recreational, industrial, natural, and agricultural purposes. The average and maximum depths are 4.5 and 7 m, respectively. The salinity of the lake decreased, and the lake became a fresh lake in few years after the dam construction, as the lake is mainly fed by the fresh water of the Ijssel River (Sollie et al., 2008). The salinity now is around 400 [mg L^{-1}] .

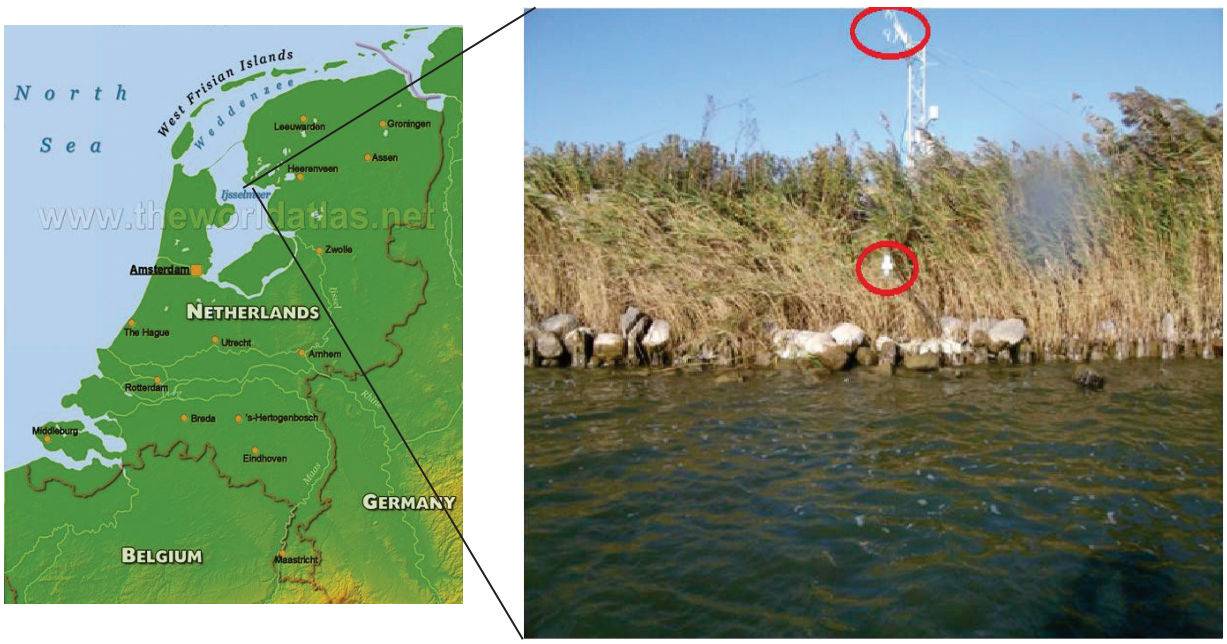

Figure 3-1.IJsselmeer Lake

3.2. Lake Tana

Lake Tana is located in the north-western part of Ethiopia. It is part of the Blue Nile basin (Figure 3-2). It covers about 3000 km² with an elevation of 1786 m above sea level. The lake is fed by over 40 rivers and streams flowing from the Simien Mountains to the North. The mean and maximum depths of the water are about 7.2 m and 14 m, respectively. It has a high economic importance as it is one of the main fish industry resources in Ethiopia. The average salinity of the lake is 143 [mg L^{-1}] (Nuru A et al., 2012).

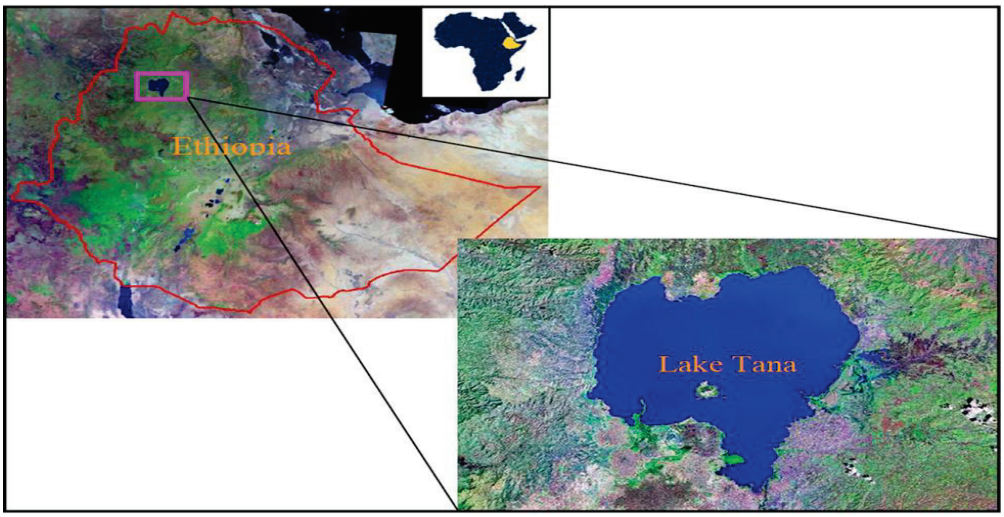

Figure 3-2.Location of Lake Tana (AbrehamKibret, 2009)

3.3. Lake Victoria

Lake Victoria is the second largest freshwater body in the world with a surface area around 68,800 km². It is bordered by three African countries: (Tanzania, Uganda, and Kenya) (Figure 3-3). It has a high economic importance. Two rivers are originated from the lake: the White Nile and the Katonga River. The mean depth of the lake is 40 m. the average salinity is 170 [mg L^{-1}] (Kaddumukasa et al., 2012).

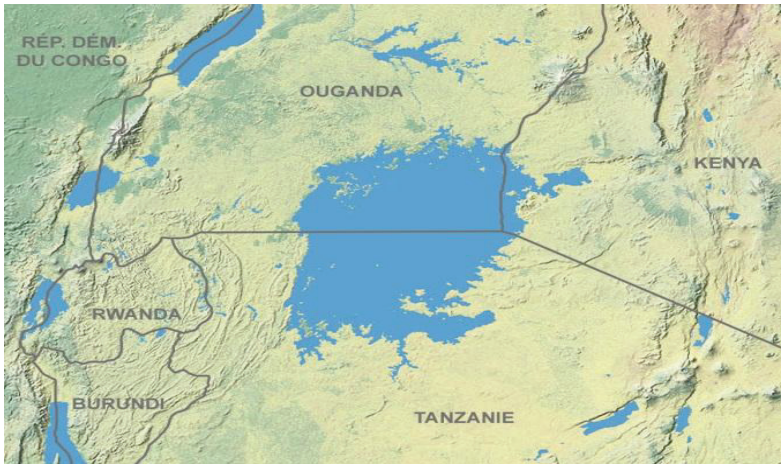

Figure 3-3.Lake Victoria

3.4. Oceans and Seas

In this study, one pixel with 1 degree spatial resolution of each area (Atlantic Ocean, Indian Ocean, Red Sea, Mediterranean Sea, and North Sea) (Figure 3-4) is used to validate the adapted SEBS model (Table 3-1). The average global salinity is 34.7 [g l^{-1}] (Williams et al., 2010).

Table 3-1 .Latitude and longitude of each study area

Study area	up-right	Down-Left
Atlantic Ocean	24^0 30` 00"N $39^0$ 30` 00"W	23^0 30` 00"N $40^0$ 30` 00"W
Indian Ocean	18^0 30` 00"S $74^0$ 30` 00"E	19^0 30` 00"S $73^0$ 30` 00"E
Mediterranean Sea	33^0 30` 00"N $26^0$ 30` 00"E	32^0 30` 00"N $25^0$ 30` 00"E
North Sea	60^0 30` 00"N $00^0$ 30` 00"E	59^0 30` 00"N $00^0$ 30` 00"W
Red Sea	18^0 30 ` 00"N $39^0$ 30` 00"E	17^0 30` 00"N $38^0$ 30` 00"E
Victoria Lake	00^0 30` 00"S $33^0$ 30` 00"E	01^0 30` 00"S $32^0$ 30` 00"E
Great Salt Lake	41^0 30` 00"N $111^0$ 45`00"W	40^0 45` 00"N $112^0$ 30` 00"W

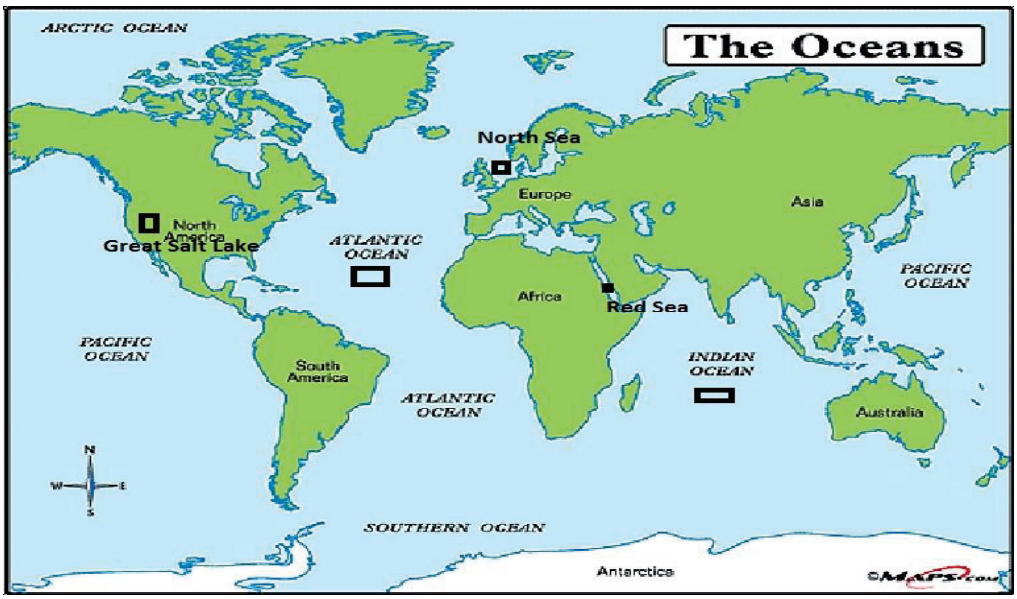

Figure 3-4.Locations of the seas and Oceans test areas

3.5. Great Salt Lake

Special attention is given for Great Salt in Utah, USA (Figure 3-5). Its area is about 5180 km^2. The lake is divided into three large bays. Gunnison Bay is located in the northwest of the lake. Its area is about 2520 km^{-2} and the salinity ranges between 280 and 300 [g l^{-1}]. Farmington Bay is located in the southeast of the lake with 260 km^{-2} area. Its salinity is up to 240 [g l^{-1}]. Gilbert Bay is located in the central of the lake. Its

area is 2400 km^{-2} approximately, and its salinity varies between 120-180 [$g\ l^{-1}$] (Wurtsbaugh et al., 2011). The lake doesn't have any outlet, so it losses water only through evaporation. Therefore, the salinity of the lake changes continuously. For Example, in a dry year, around 10% increase in the lake's salinity occurred between September 2006 and August 2007(Diaz et al., 2009). The ECMWF grid doesn't cover the lake only, but the ground represents around 20% of the pixel.

Figure 3-5. Great Salt Lake

4. DATA SETS

4.1. In-situ measurements

Hydro-meteorological data are the main input to study the components of the water balance system of an area. As a part of this research, an in-situ data collection was implemented in the period between 11st October and 14th November 2012 on the Ijsselmeer Lake. Different meteorological parameters were measured over the water surface, as described in the following sub-sections.

4.1.1. Instruments

The description of the instruments used in the field work is presented in the following:

4.1.1.1. Radiations

The CNR1 radiation sensor (Figure 4-1) was used to measure the four components of radiations (incoming and outgoing shortwave and longwave radiations). Solar and thermal infrared radiation can be detected separately by this instrument. The spectral range of the measurement is between 0.3 to 50 μm. This range covers both the shortwave radiation from 0.3 to 3 μm, and the thermal infrared radiation between 5 and 50 μm. Two CM3 pyranometers are used in the instrument to measure the incoming and the reflected solar radiation. This enables the user to estimate the albedo value. For measuring the far infrared radiation, two CG3 pyregeometers are used. One measures the incoming longwave radiation from the sky, and other measures the outgoing radiations from the surface.

Figure 4-1.CNR1 net radiometer sensor

4.1.1.2. Air temperature and relative humidity

The HMP45C relative humidity-temperature probe was used during the field work. This probe is produced by Campbell Scientific. The probe must be housed inside a radiation shield to prevent the solar radiation load effect. The working range of the measurements is between $\pm 50°C$ and from 0 to 100% for the temperature and the relative humidity, respectively. It gives high-accuracy measurements about $\pm$ 3°c for temperature and ± 0.2% for the relative humidity.

4.1.1.3. Lake Temperature

The TMC6-HOBO probe was used in estimation the vertical temperature profile at different depths in the water. Temperature sensors are used with HOBO external – channel data loggers. The temperature sensors were calibrated before the field work implementation.

4.1.1.4. Eddy co-variance

The CSAT3 instrument was used for measuring the heat fluxes (Figure 4-2). It is a three – dimensional sonic anemometer, as it measures the wind speed and the speed of sound on three non - orthogonal axes. The sonic temperature and orthogonal wind speed are computed using these measurements. The anometer point was in the same direction of the prevailing wind direction of the lake to minimize the contamination of the data by the anometer's structure. The technical specification of the CSAT3 can be summarized as follows:

- Dynamic range of temperature: -30 ℃ to + 50 ℃
- Sound speed: 300 to 366 ms^{-1}
- No data can be obtained during rain.

Figure 4-2.CSAT 3-D sonic radiometer

4.1.2. Data collection

The eddy-covariance sensor was installed at 3 m height. Other instruments, including air temperature, and relative humidity were fixed on the same tower at 2m height. The tower was located about 3 m far from the water along the lake shore. This value is less than the offset value of the contribution probability function. The radiation sensors were installed at 1.5 m height above the water surface, and 4 m away from the land. The water temperature profile sensors were fixed to a special float wood, which permitted the thermometers to move vertically with the waves without change the depths and height of the temperature sensors. The water temperature profile instrument was fixed on a definite point in the lake using two masses in the bottom (Figure 4-3).

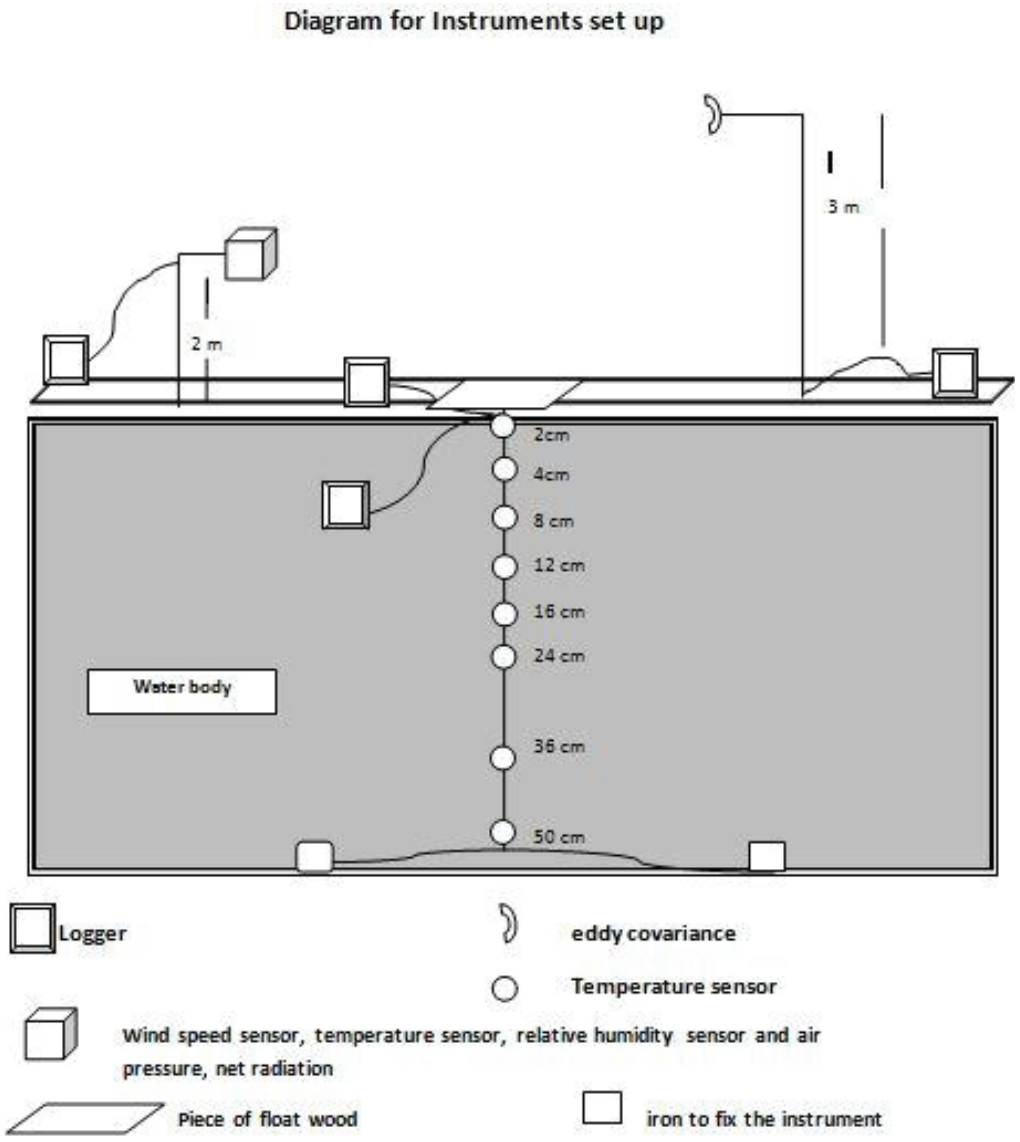

Figure 4-3.Instruments set up

4.1.3. Data pre-processing

All the measured values, including the four components of radiations, air temperature, and relative humidity are averaged over 30 minutes interval. Due to technical problems, the water temperature measurements were lost. Therefore, the water surface temperature is calculated by inversing the Stefan-Boltzmann equation.

Two software tools (Eddypro and AltEddy) are used to process the eddy co-variance raw data to ensure the data quality. AltEddy tool has been developed by Alterra group, Wagenigen University, The Netherlands. Eddypro is free software developed by Li-CorCompany. The two tools are used to validate the results and reduce the errors. They estimate the turbulent heat fluxes, friction wind, mean wind speed, sonic temperature and wind variances.

- The first step in the eddy co- variance processing procedures is downloading the data from the logger.
- Then the data convert from binary version to ASCII format and unknown (Nan) data records are removed.
- Thirdly, an interval file for the data is created (30 minutes) and the metadata of the instrument, tower installation, nature of the region and the raw data files are entered into the software.
- After that, to improve the quality of the data and remove the potential error, the accepted data values is limited to upper and lower boundaries that should not be exceeded (Table 4-1).
- In addition, spiked values produced as a result of random electronic errors, biophysical reasons (e.g. changes in the footprint or fast change in the turbulence), and instrumental problems (like formation of water droplets in the anometer) are also be removed (Papale et al., 2006). These errors are determined as a deviation from the mean (Equation 18) by more than:

$$\frac{\mathrm{MSPI}}{100}\,(\mathrm{U.L}-\mathrm{L.L}) \qquad \text{Equation 18}$$

Where

MSPI : degree of deviation from the mean as a percentage.

(U. L-L. L) : difference between the upper and lower limits.

Table 4-1. Limits of eddy covariance processing (Rwasoka et al., 2010)

Variable	lower limit	upper limit	Alteddy code
Sonic U lower limit in m/s	-30		LILO (a)
Sonic U upper limit in m/s		30	LILH (a)
Sonic w lower limit in m/s	-30		LILO (b)
Sonic w upper limit in m/s		30	LILH (b)
Sonic v lower limit in m/s	-30		LILO (c)
Sonic v upper limit in m/s		30	LILH (c)
Sonic T lower limit in Kelvin	263		LILO (d)
Sonic T upper limit in Kelvin		313.15	LILH (d)
LICOR 7500 H_2o lower limit in mmol/m3	0		LILO (e)
LICOR 7500 H_2o upper limit in mmol/m3		1200	LILH (e)

- Finally, the data is limited to the lake heat fluxes data when the wind direction ranges between 200-280°. The field work data is divided into two equal parts. One is used to estimate the roughness heights for momentum and heat transfer by (S. M. Liu et al., 2007) model. The second dataset is used to validate the SEBS sensible heat part over Ijsselmeer Lake using the estimated roughness heights parameters.

(Vesala et al., 2008) defined the footprint as "the field of view of the flux sensor". The footprint is the area around of the instrument (mostly up wind) that can influence a measured flux at a particular location. Several methods have been developed to determine the footprint (Schmid, 1997); (Schotanus et al., 1983); (Liu et al., 2001; Vesala et al., 2008). In this study, the model of (Rwasoka et al., 2010) was used to determine the flux footprint of the eddy co variance tower. Measurement height, surface roughness, and

the atmospheric stability parameters are required in implementation the model. In addition, the EddyPro software estimated the footprint using (Kljun et al., 2004) model during the data processing.

4.2. ECMWF data

The ECMWF products are provided by the European Centre for Medium range Weather Forecasts intergovernmental organization. This organization is supported by 34 countries. Different meteorological products such as wind speed, air temperature, surface temperature and evaporation maps are developed using numerical models and collected data from various regions around the world. The products can be downloaded in various spatial resolutions in netcdf format via website: http://data-portal.ecmwf.int/.
Panoply software is freely available for processing the data via the website: http://www.giss.nasa.gov/tools/panoply/download_gen.html, also GIS Software supported by ITC is used in the processing.
To avoid the errors due to the uncertainty of the atmospheric input parameters, the ECMWF meteorological data was used as input parameters and the heat fluxes products were used to validate the adapted SEBS model outputs.

4.3. Historic data

The data of Lake Tana was provided by Dr. Christiaan van der Tol (ITC, University of Twente). It was collected during the period of 15-9-2011 to 16-9-2011. The data includes temperature profile at different depths in the water and air, wind speed, relative humidity, water surface temperature and net radiation components.

4.4. Satellite data

The European space agency's (ESA) Envisat satellite crossed the equator on the morning at (10:00 local time). One of the on-board instruments is the Advanced Along-Track Scanning Radiometer (AATSR), a visible, near-infrared and thermal sensor. The main task of this instrument is providing accurate data concerning global sea-surface temperature using multi-channel imaging radiometer. The AATSR is a visible, near-infrared and thermal sensor. Along-track scanning technique was used, which observe the same point on the globe from two different angles. It uses three infrared channels 3.7 μm, 10.85 μm and 12.5 μm to estimate the temperature of the surface. The 3.7 μm channel is only used at night, owing to the contamination by reflected solar at daytime. This radiometer scans conically making two independent observations (forward and nadir view). The six independent observations of the three channels improve the atmospheric correction process efficiency. Consequently, the accuracy of measurement is better than 0.3°k (Llewellyn-Jones et al., 2012).

The AATSR products can be downloaded through the ESA website with 1 Km spatial resolution and high spatial coverage.

5. RESULTS AND DISCUSSION

5.1. SEBS to fresh water

5.1.1. Water heat flux

The equilibrium temperature model has been applied over different areas. The results were compared with the ECMWF water heat flux (calculated as a residual of energy equation) and are shown (Table 5-1) To investigate the behaviour of the model under different atmospheric conditions, several plots are created (Figure 5-1), (Figure 5-2) and (Figure 5-3).

Table 5-1.a comparison of water heat flux between ETM and ECMWF models

	Indian Ocean		Atlantic Ocean		Mediterranean Sea		North Sea		Red Sea	
	ETM	ECMWF	ETM	ECMWF	ETM	ECMWF	ETM	ECMWF	ETM	ECMWF
n	1005	1005	1005	1005	1005	1005	1005	1005	974	974
Average [W m^{-2}]	126.5	120.0	53.7	55.7	507.5	513.8	101.1	147.7	573.3	542.7
STD [W m^{-2}]	180.5	175.1	131.6	131.8	284.8	253.8	284.2	252.5	132.5	136.3
RMSE [W m^{-2}]	32.2		26.5		49.6		68.5		42.1	
rRMSE (%)	4.8		4.3		5.2		8.5		6.4	

ETM: Equilibrium Temperature Model

STD: Standard deviation

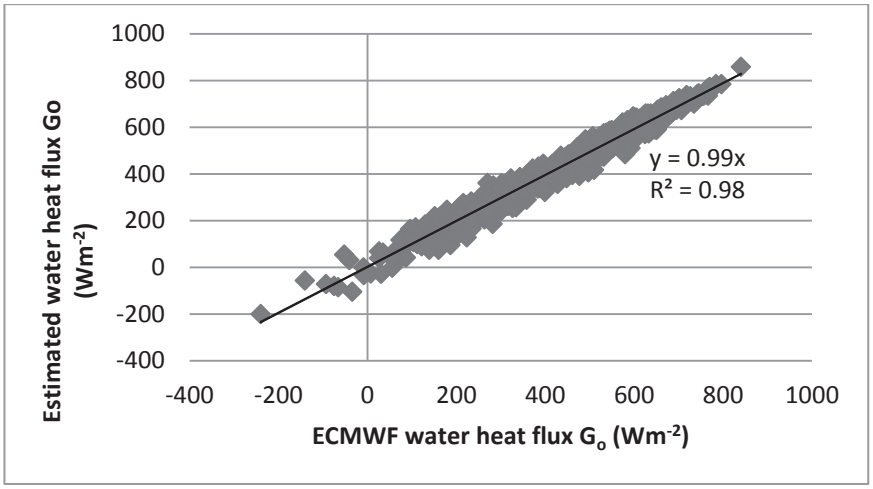

Figure 5-1. comparison of water heat flux between ETM and ECMWF

over Atlantic Ocean test area at 18:00 GMT in the period (January 2010 – September 2012)

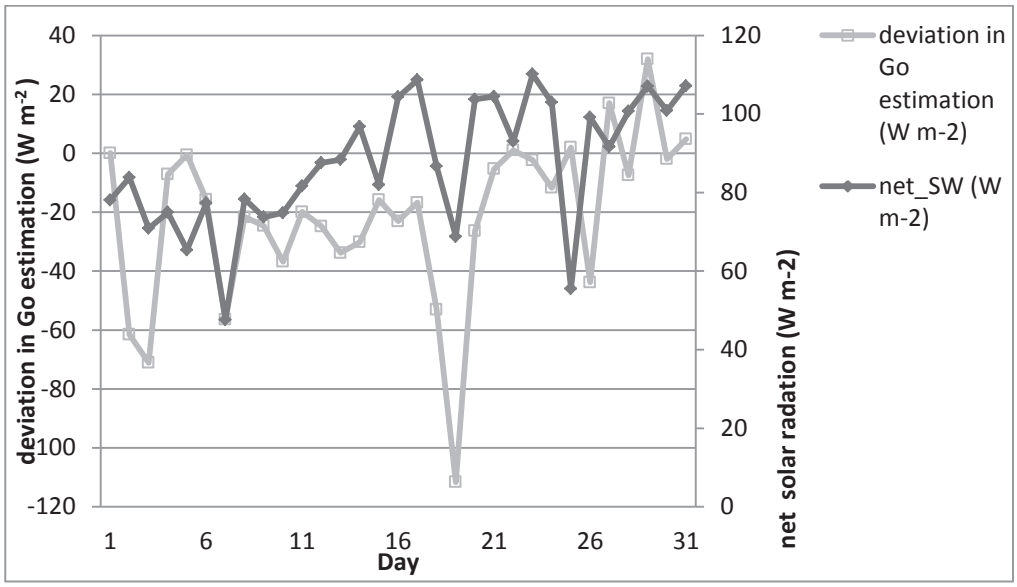

Figure 5-2. correlation between water heat flux estimation deviation and net solar radiation over Atlantic Ocean test area at 21:00 GMT on January 2010

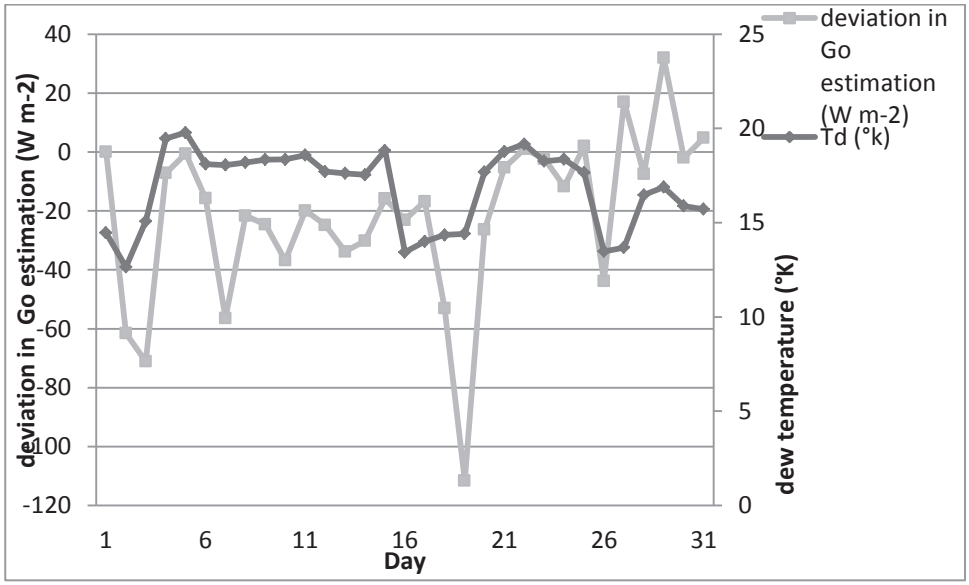

Figure 5-3.correlation between water heat flux estimation error and dew temperature over Atlantic Ocean test area at 21:00 GMT on January 2010

It can be observed from (Figure 5-1) that the estimated water heat flux follow the same behaviour of ECMWF data, the deviation in water heat estimation is mostly confined to 50 [W m^{-2}]. The equilibrium temperature model exhibits underestimation when net shortwave radiation and dew temperature are low (Figure 5-2) and (Figure 5-3).

The thermal exchange coefficient (β) is stable during the day (Figure 5-4). It mostly ranges between 20–60 [W m^{-2} $^{\circ}c^{-1}$]. The average of the daily standard deviation over Atlantic and Indian Ocean are 2 [W m^{-2} $^{\circ}c^{-1}$] and 1.66 [W m^{-2} $^{\circ}c^{-1}$], and the average daily variances are 5.57 [W m^{-2} $^{\circ}c^{-1}$] and 3.86 [W m^{-2} $^{\circ}c^{-1}$],

respectively. Thermal exchange coefficient describes how sensible heat, latent heat and longwave radiation responds to the variations in water surface temperature. Sensible and latent heat are mostly constant during the day. In addition, the net longwave radiation is stable throughout the day over the water surface with limited variation during night time (de Szoeke et al., 2010). Therefore the thermal exchange coefficient follows the same stability behaviour over the day.

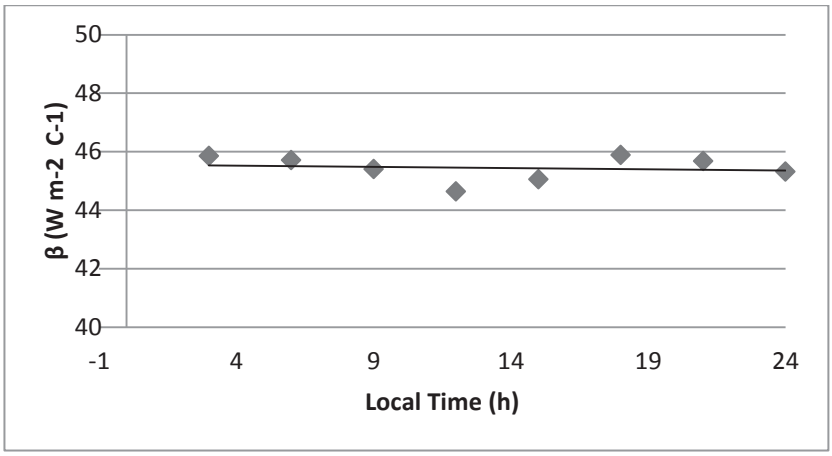

Figure 5-4.the diurnal stability of thermal exchange coefficient

over Atlantic Ocean test area, 1st January 2010

The calculated equilibrium temperature (T_e) follows the same behaviour of the water heat flux and the incoming solar radiation over the day period; therefore it takes a diurnal convex downward shape (Figure 5-5). From this point of view, we can conclude that the daily average of the equilibrium temperature is approximately equal the mid-day equilibrium temperature (Figure 5-6).

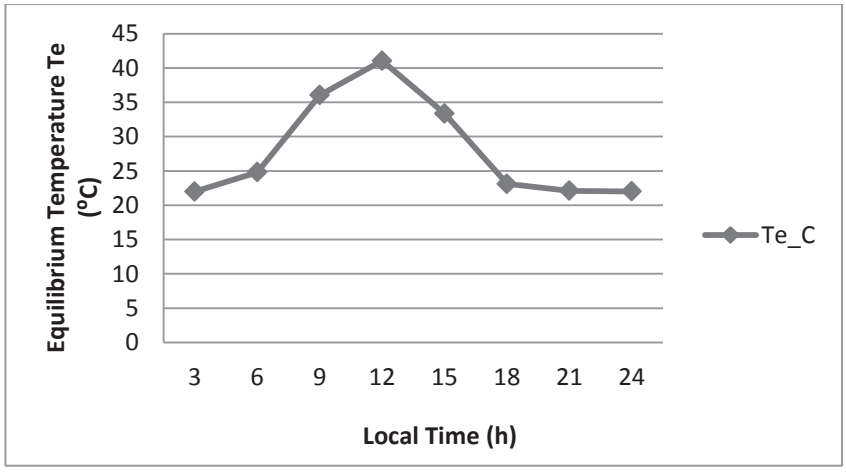

Figure 5-5.the diurnal equilibrium temperature

over Indian Ocean, 1thJanuary 2010

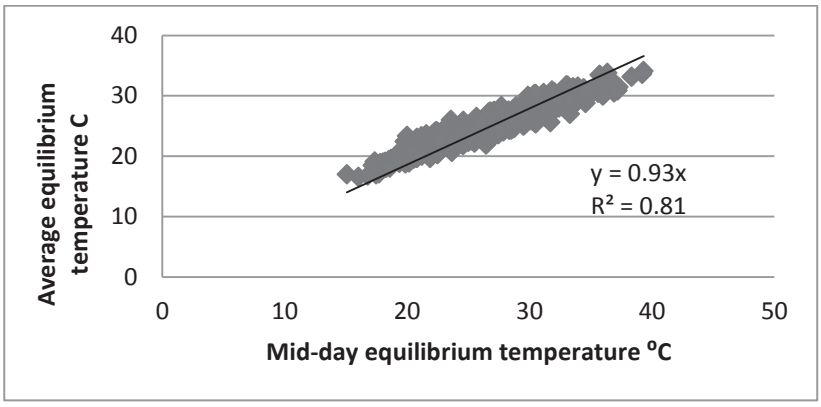

Figure 5-6.agreement between mid-day and average equilibrium temperature (°c)

over Atlantic Ocean test area in the period between 1st January and 30th September 2012

During the field work, the data of vertical temperature profile had been lost, so the equilibrium temperature model was used to estimate the water heat flux over IJsselmeer Lake. The results were validated against the water heat flux results calculated as a residual of the energy balance equation. The results show a weak correlation with R-square value 0.23 between the model and the measurements. This may be attributing to many reasons:

1. Firstly, very low incoming shortwave radiation and dew temperature values, where the model is relatively inaccurate and a high underestimation can happen.
2. Moreover, there is a difference in the spatial coverage of the eddy covariance sensor and the other instruments.
3. Finally, the influence of the lake bottom on the net radiation value should be considered as the albedo value is 0.35. This is considered much higher than the common water surface albedo, which ranges between (0.05- 0.11) (Abreham Kibret, 2009). This is due to the effect of the lake bottom as the lake depth in this area is around 50 cm.

Many factors influence the water heat flux value. Water heat flux relates to the temperature gradient and the wind speed in an inverse way, as these atmospheric parameters represent the driving force for the sensible heat and latent heat fluxes. The correlation between water heat flux and temperature gradient is between 0.3-0.45, as well as the correlation between water heat flux and wind speed is between 0.2-0.4.

The net radiation has the greatest effect on the water heat flux value. We observe that the ratio between the water heat flux and net radiation increases in a logarithmic way with the net radiation (Figure 5-7). This statement incompatibles with (Jia et al., 2009a), which assumes that the ratio between water heat flux and net radiation is 0.5. These logarithmic equations parameters change in a spatial and temporal ways (Figure 5-8) and (Figure 5-9). The temporal and spatial differences in the value of water heat flux and net radiation ratio is due to the different forms of water heat flux as mentioned above (Meehl, 1984). Moreover, the salinity stratification plays a great role in the estimation of the convection layer and the amount of heat store in the water body. It limits the convection layer in the Pacific Ocean to 150 m or less, although the Atlantic Ocean convection layer is around 300 m or more (Meehl, 1984). We observe that when the net radiation is higher than 300 [W m^{-2}]; the ratio between water heat flux and net radiation is mostly higher than 0.6. This statement is incompatible with (Burba et al., 1999), which states that 45-60% of the net radiation during the day is consumed in water heat flux term. In the same manner; this ratio also displays a logarithmic behaviour with the net shortwave radiation (Figure 5-10).

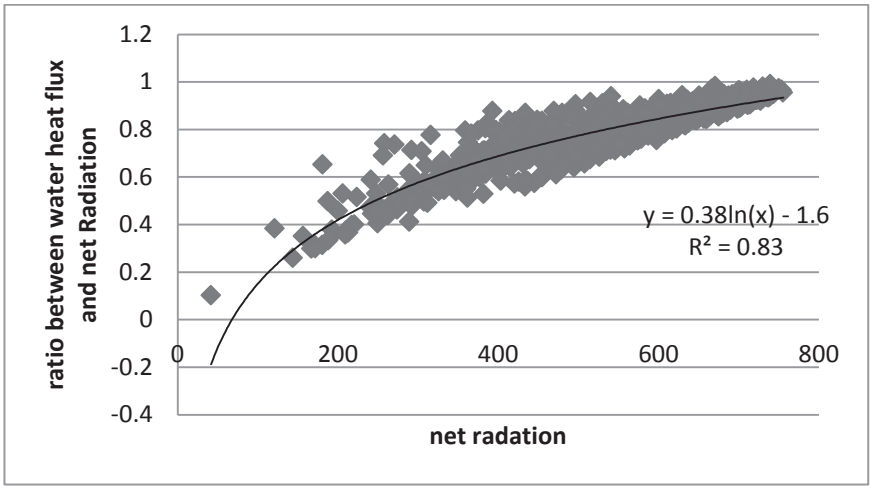

Figure 5-7. relationship between net radiation and the ratio of water heat flux to net radiation over Red Sea (January 2008 - December 2009)

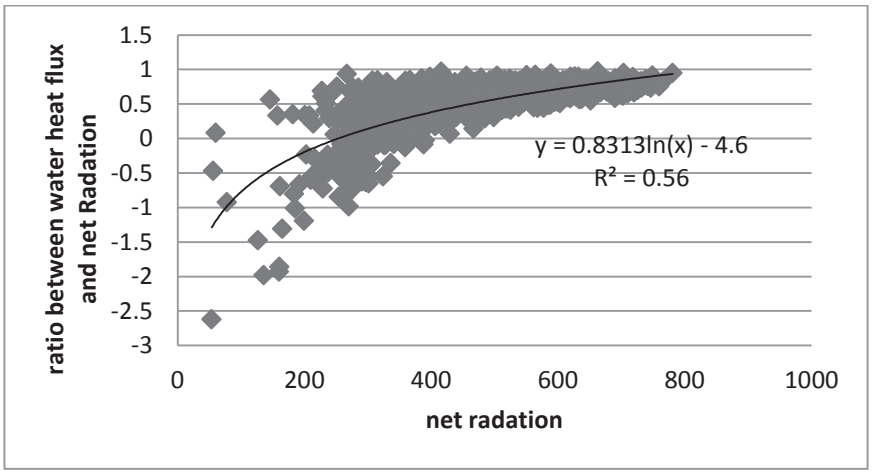

Figure 5-8. relationship between net radiation and the ratio of water heat flux to net radiation over Indian Ocean (January2008 -December 2009)

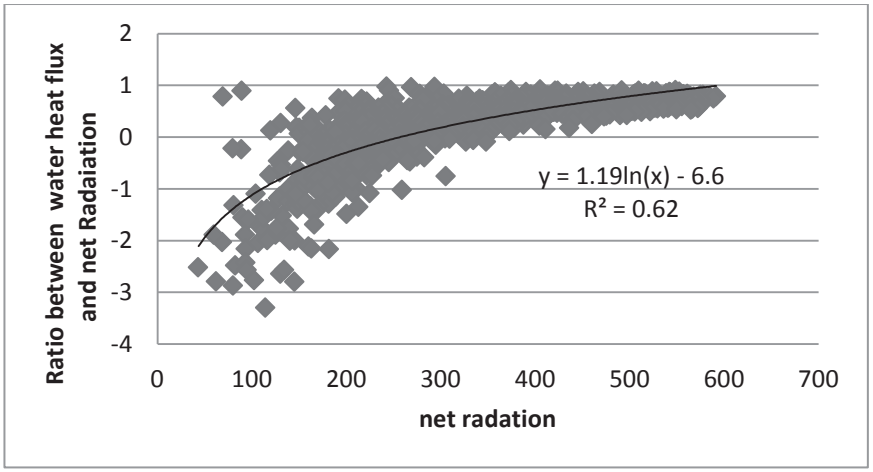

Figure 5-9. relationship between net radiation and the ratio of water heat flux to net radiation over Indian Ocean (January2010 - September 2012)

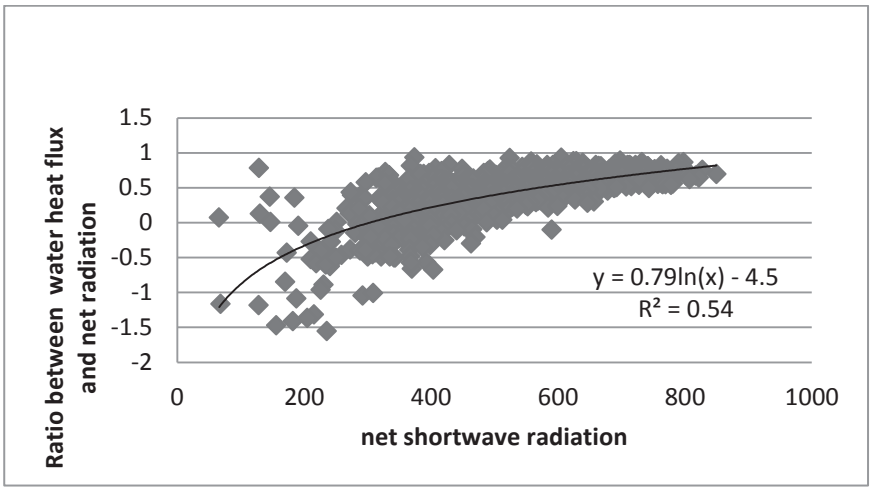

Figure 5-10. relationship between net solar radiation and the ratio of water heat flux to net radiation over Indian Ocean (January 2010 - September 2012)

5.1.1.1. Daily water heat flux

In contrast to (Abreham Kibret, 2009), this study shows that the daily water heat flux doesn't equal zero, and the energy gained during the daytime doesn't release totally during the night time (Figure 5-11). This can be explained it terms of convectional and conduction transfer of the heat through the water body

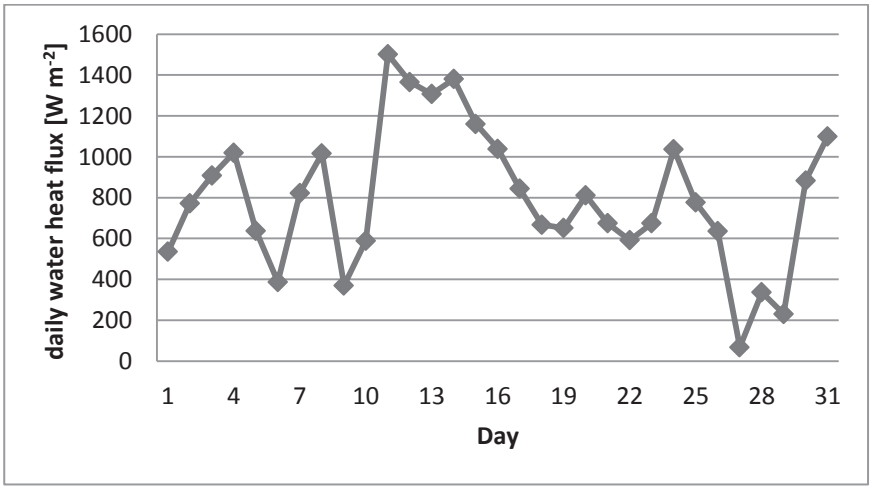

Figure 5-11.the daily water heat flux in January 2010 over Indian Ocean

5.1.1.2. Water heat flux Error analysis

A high error in the water heat flux estimation will affect largely the performance of SEBS model, as it is the major component in water energy balance system. Therefore, it is very important to know the sensitivity of the estimated value to each input parameter. Using the average of water surface temperature 25.08 ˚c, wind Speed 6.36 [m s^{-1}], dew temperature 19.03 ˚c and net solar radiation 277.48 [W m^{-2}] of the Atlantic Ocean data, the sensitivity of each parameter is determined as $\Delta G_o = -47\,\Delta T_0$, $\Delta G_o = 38\,\Delta T_d$ and $\Delta G_o = -35\,\Delta u$, as well as the sensitivity of the model to the net solar radiation equals unity. In this regard, it can be shown that the water heat flux is more sensitive to the surface water temperature than the other parameters (Table 5-2). If the water surface temperature and the wind speed increase by 1%, the

water heat flux value will underestimate about 52% and 10%, respectively. On the other hand, 1% error in dew temperature measurement will overestimate the water heat flux value by 32%. In conclusion, the most – to – least effectual parameters on the water heat flux value are water surface temperature, dew temperature, wind speed, net solar radiation.

Table 5-2.the sensitivity of estimated water heat flux to its input atmospheric parameters using direct and linear error model

	Nominal	Bias	Ratio	Direct ΔGo	Linear ΔGo	Direct ΔGo/Go	Linear ΔGo/Go	Exact (%)	Linear (%)
water surface temperature[°C]	25.08	0.25	0.01	-11.78	-11.73	-0.52	-0.52	-52	-52
dew temperature [°C]	19.03	0.19	0.01	7.23	7.20	0.32	0.32	32	32
wind speed [m s^{-1}]	6.36	0.06	0.01	2.20	-2.20	-0.10	-0.10	-9.8	-9.7
All				-6.76	-6.73	-0.30	-0.30	-29.9	-30

Negative value indicates underestimation process

5.1.2. Sensible heat

While on land sensible heat takes a lot of the available energy, above water surface values are a lot less (almost less than 20% of the available energy), as can be seen in (Figure 5-12). Aerodynamic resistance plays a great role to keep the sensible heat energy in a very limited range. Eddy covariance data was used to estimate the aerodynamic resistance parameters, including the roughness of momentum and heat transfer. It is shown that the aerodynamic resistance of the water surface relates to the wind speed in an inverse exponential way. Therefore, an increase in the wind speed value will lead to decrease the aerodynamic resistance of water. Above 3 [m s^{-1}] wind speed, the aerodynamic resistance over water surfaces ranges mostly between 50 and 200 [s m^{-1}], resulted in low sensible heat fluxes (Figure 5-13).

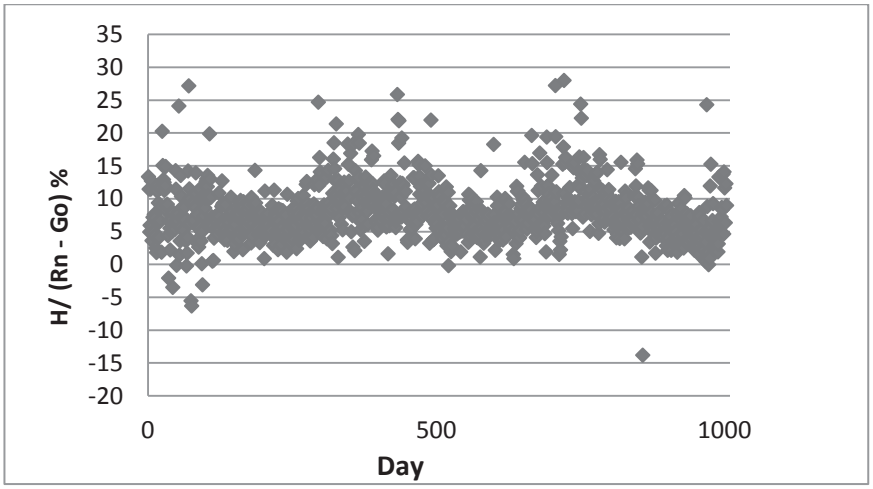

Figure 5-12.the ratio between sensible and available energy (%) over Atlantic Ocean (January 2010 – September 2012)

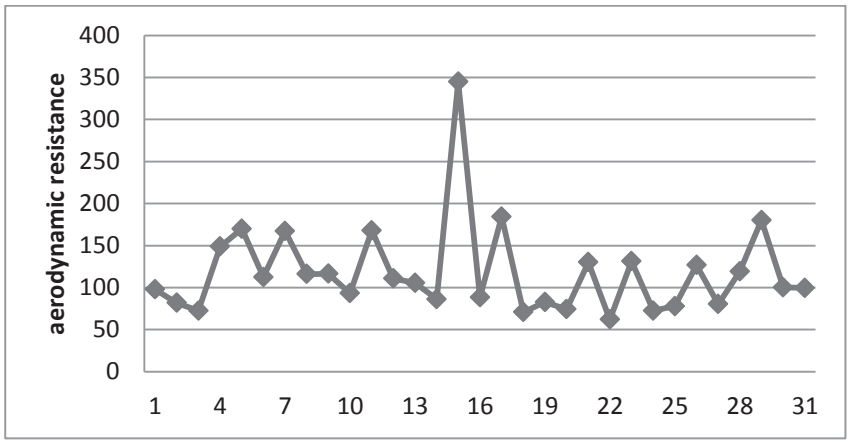

Figure 5-13.the aerodynamic resistance of heat transfer over Mediterranean Sea

(January 2010)

5.1.2.1. Eddy covariance and flux footprint

The data collected during the field work period between (11-10-2012 and 14-11-2012) were used to estimate the roughness lengths of momentum and heat transfer. Firstly, the results of the two tools (Alteddy and EddyPro) were compared, to check the processing quality. It is found that the deviation is mostly confined within around ± 3 [W m^{-2}] and the reproducibility is 2.7 [W m^{-2}], which indicates a high agreement between them (Figure 5-14).

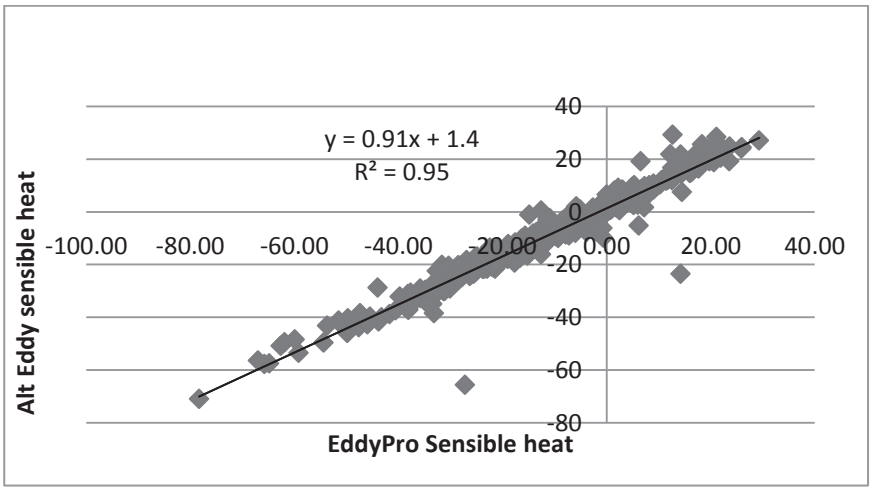

Figure 5-14.a comparison between Alteddy and Eddypro sensible heat

on IJsselmeer Lake in the period between 11-10-2012 and 26-10-2012

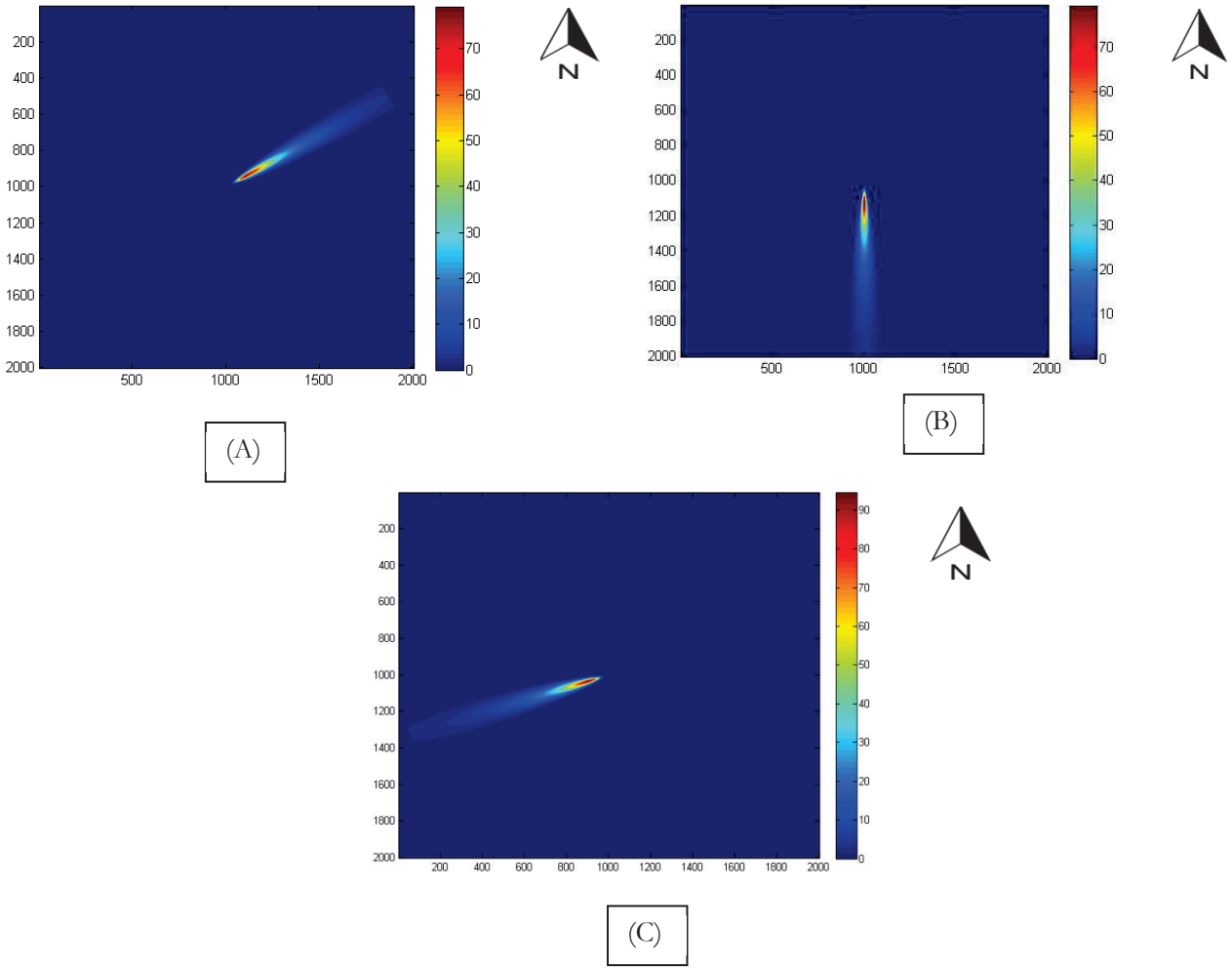

Figure 5-15.the footprint contribution probability areas

(A) the contribution area from the land in October 26, 2012. (B) the contribution area from the land and the Lake in October 12, 2012. (C) the contribution area from the Lake in October 14, 2012.

As explained in chapter (4.1.3), two models were used to estimate the footprint fluxes of eddy covariance measurements. Figure (5-15) represents different contribution areas from the land (a), the lake and the land (b), and the lake (c). This research is just concerned with the data from the lake. The different colours represent the different contribution probability for each pixel. The highest contribution pixel has red colour, and the lowest is the blue pixel. The average footprint of 90% contribution probability calculated by the EddyPro is 211 m on 13rd October 2012 (Table 5-3).

Table 5-3.the footprint contribution probability in October 13, 2012

model	x_peak	x_offset	x_10%	x_30%	x_50%	x_70%	x_90%
--	[m]	[m]	[m]	[m]	[m]	[m]	[m]
kljun_04	77.2	-11.7	26.5	66.0	100.6	141.1	211.4

5.1.2.2. Roughness height for momentum transfer

The model from (Tanny et al., 2008) was used to estimate the roughness of momentum transfer (Z_{om}) over a water surface. It is a function of friction velocity, which was estimated by the eddy covariance. For the wind speed ranges between 0.16 and 12 [m s^{-1}], the roughness height for momentum transfer is 0.0002 m. This indicates that the theoretical level of momentum flux exchange between the water body and the atmosphere is very near to the water surface. This value has been validated on various study areas and under different atmospheric stability conditions and atmospheric parameters' values as explained later.

5.1.2.3. Roughness height for heat transfer

The model from (S. M. Liu et al., 2007) was applied to estimate the roughness height for heat transfer (Z_{oh}) over a water surface. The sensible heat, friction velocity and Monin-Obukhov length were measured by the eddy covariance. The roughness height for heat transfer parameter over a water surface was estimated to be 0.0001 m, where the sensible heat ranges between -70 [W m^{-2}] and 30 [W m^{-2}]. The estimated roughness heights parameters were used to estimate the sensible heat over IJsselmeer Lake using SEBS model in the period of 11-26 October 2012. The results show similarity between SEBS heat fluxes and the eddy covariance heat fluxes data (Figure 5-16) with RMSE 9.0 [W m^{-2}] and R-square 0.72.

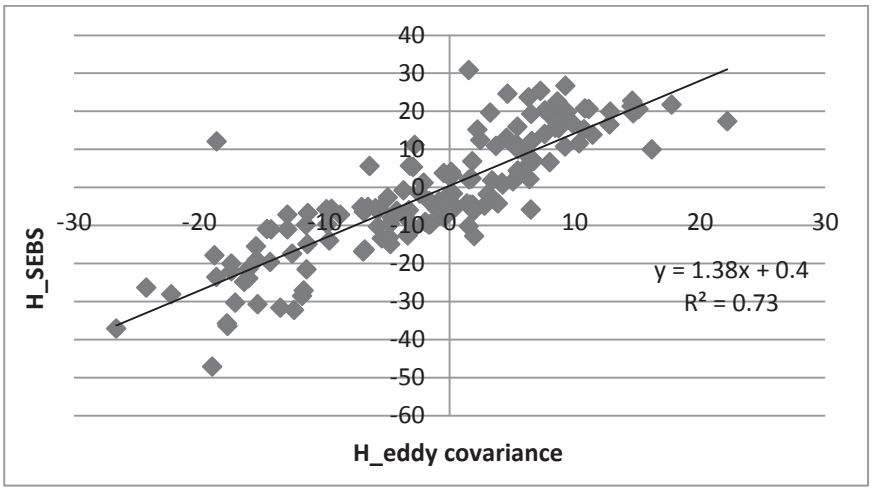

Figure 5-16.a comparison between the measurements and SEBS sensible heat over IJsselmeer Lake

The low difference between the roughness height for momentum transfer and its counterpart for heat transfer is reflected in the KB^{-1} value. It is estimated to be 0.3 over water surfaces. In the same regard, it is apparent that the roughness height for heat transfer is less than for momentum transfer, that means the level of heat source is lower than the momentum sink level; therefore, the aerodynamic resistance of heat transfer is larger than of momentum transfer (Owen et al., 1963; Stewart et al., 1973; Thom, 1972). Although (S. M. Liu et al., 2007) states that the poorest estimation of sensible heat flux takes place when the difference between the roughness lengths is low, SEBS model over a water surface exhibits a good estimation of the sensible heat. This is due to the iteration process of the similarity relationship equations between the sensible heat, friction velocity and Monin-Obukhov length, which plays a great role in the accurate estimation of these parameters. In addition, this model is less sensitive to the roughness parameters over water surfaces than to the atmospheric parameters (this part will be explained in more details in the next chapter).

5.1.2.4. Sensible heat error analysis

The sensible heat flux is more sensitive to the atmospheric conditions than to the aerodynamic resistance of the water surface. The direct method was used to estimate its sensitivity to each input atmospheric parameter over the Atlantic Ocean. (Figure 5-17) shows that the temperature gradient is the main motivation force of the sensible heat over water surfaces. The sensitivity of sensible heat to the wind speed is less than to the temperature gradient and higher than to aerodynamic resistance parameters. (Figure 5-18) illustrates that the influence of roughness of momentum and heat on the sensible heat doesn't exceed 6.5% when the roughness parameters are within 50% of their actual values.

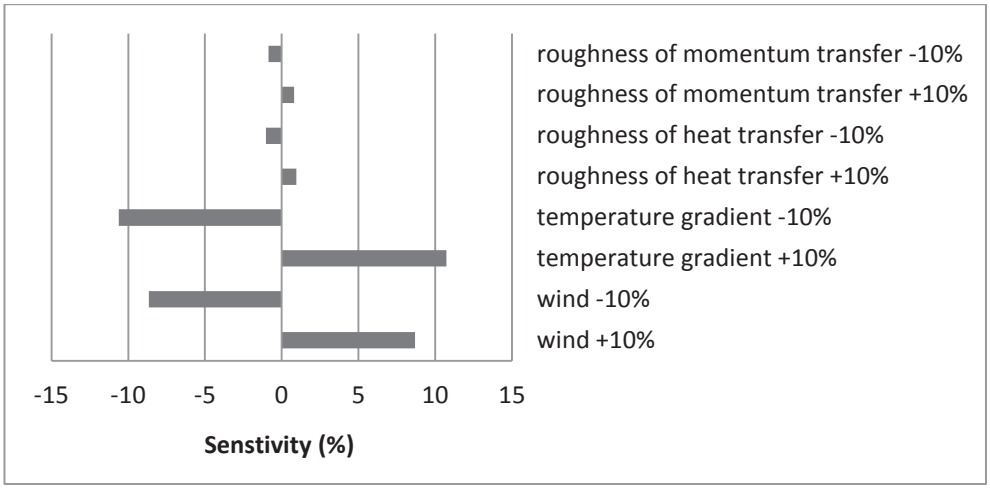

Figure 5-17.the sensitivity of estimated sensible heat to its input parameters

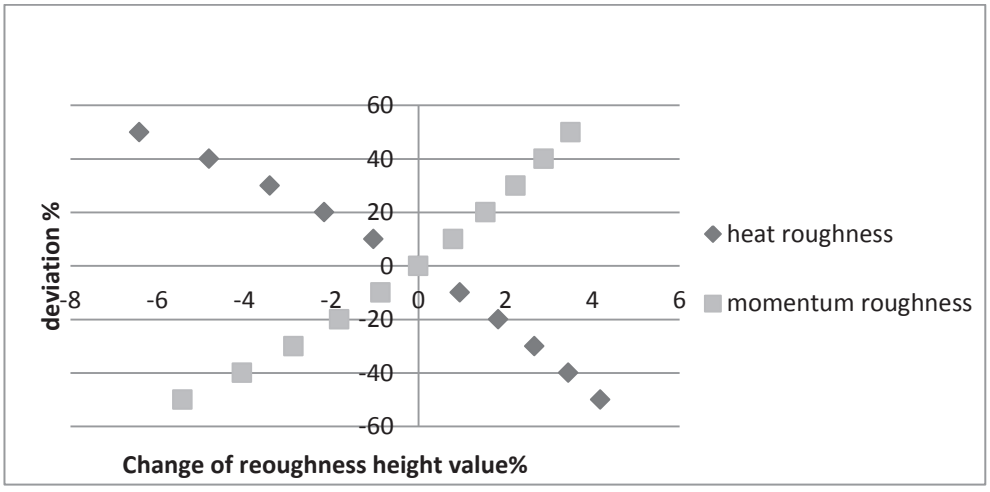

Figure 5-18.sensitivity of estimated sensible heat to roughness heights for momentum and heat transfer

5.1.3. Daily evaporation

The evaporative fraction is a diagnostic property of the heat fluxes and the daily evaporation processes. It was investigated by (Li et al., 2008) that the evaporative fraction is not stable during the day over the land, if the net radiation is less than 200 [W m^{-2}]. Over Ocean however, the water heat flux releases energy to

keep the latent and sensible heat over a water surface in a stable state (Manrique Suñén et al., 2012), therefore, the ratio between latent heat and available energy is stable during the day (Figure 5-19)

. It is found that the average daily standard deviation of the evaporative fraction over Atlantic Ocean in the period between January 2010 and September 2012 is 0.05 [W m^{-2}], which refers to the stability of the evaporative fraction under different atmospheric conditions and parameters. This finding is illustrated by the evaporative fraction over the Mediterranean Sea in (Figure 5-19). It is concluded that the evaporative fraction at overpass time of the satellite can be used to upscale evaporation rate estimation from instantaneous to a daily basis.

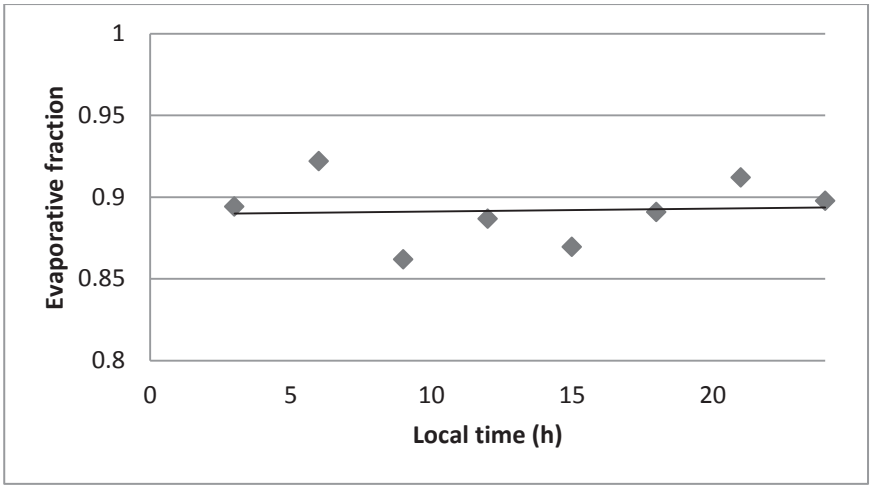

Figure 5-19.stability of evaporative fraction over the day period

over Mediterranean Sea on 1st January 2010

The evaporative fraction over water surfaces has mostly high value, as most of the available energy is converted to latent heat. The histogram (Figure 5-20) illustrates that the evaporative fraction ranges mostly between 0.8 - 1.0 under unstable conditions, and 1.0 – 1.2 under stable conditions when the sensible heat has a negative value. This range indicates that the latent heat under stable conditions dissipates energy from the stored heat in water body. In the same regard, the ratio between the latent heat and the available energy at the surface is mostly higher than 0.8 (Figure 5-21). That means more than 80% of the available energy at the water surface during the day is used in the evaporation process.

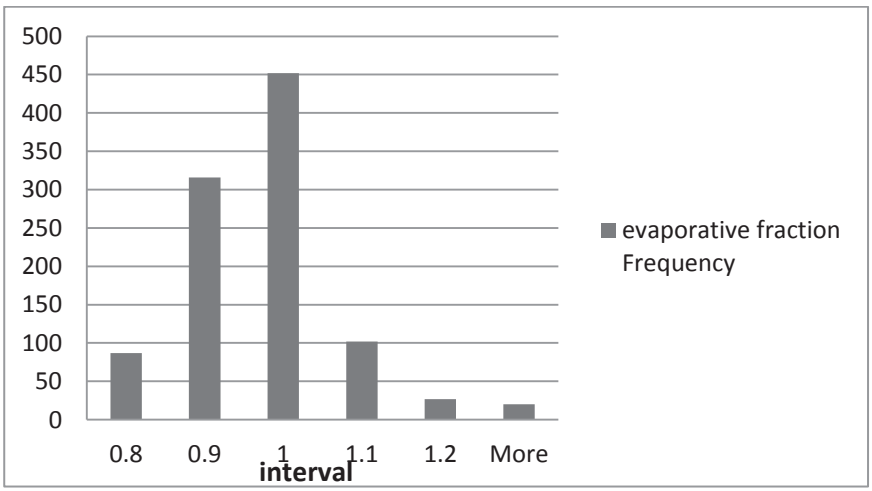

Figure 5-20.a histogram of the evaporative fraction over Mediterranean Sea

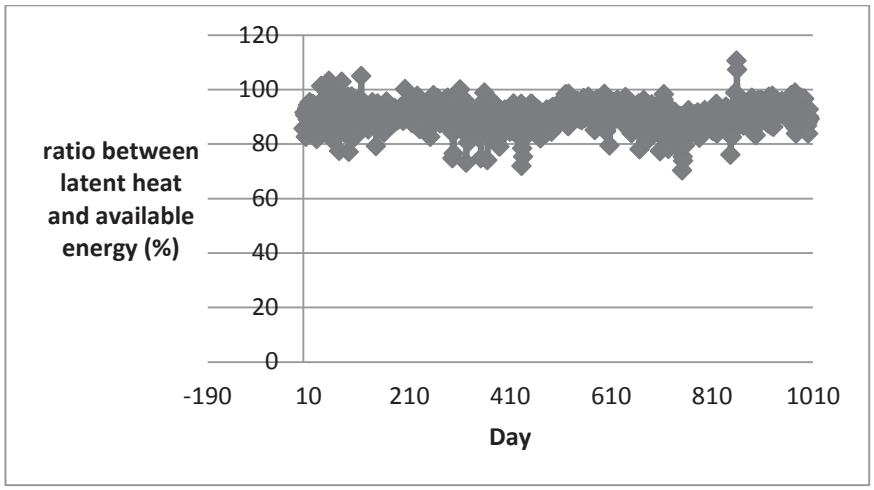

Figure 5-21. ratio between latent heat and available energy

over Atlantic Ocean in the period of (January 2010-September 2012)

SEBS uses the evaporative fraction and the daily available energy to upscale the latent heat from instantaneous to a daily basis, where the daily ground heat flux can be considered zero. Unfortunately, the daily water heat flux isn't exactly zero. According to (Manrique Suñén et al., 2012), the sensible and latent heat fluxes are stable during the day; therefore, the available energy follows a constant behaviour during the day. This character was investigated over various study areas and under different atmospheric conditions (Figure 5-22). We can conclude that the available energy and the evaporative fraction are stable during the day; therefore SEBS model is valid over water surface to upscale the evaporation rate from instantaneous to daily basis.

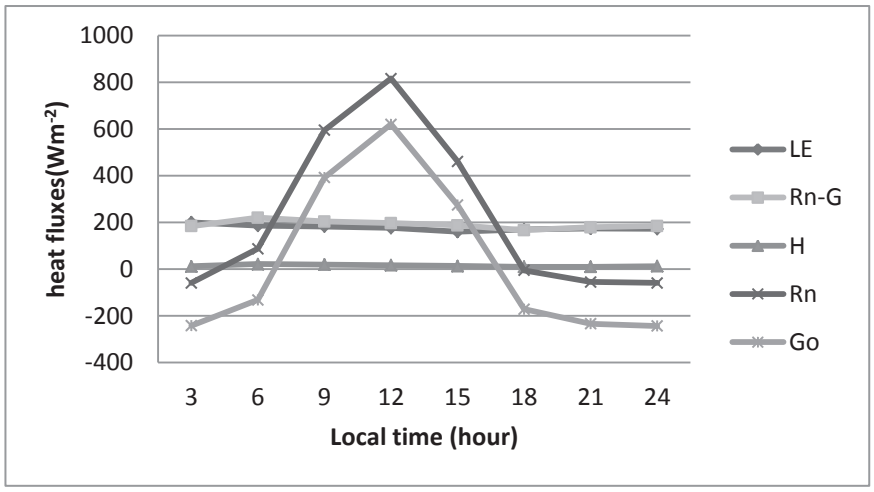

Figure 5-22.heat fluxes and available energy over Indian Ocean

1st January 2010

5.1.4. Validation of the adapted SEBS model over freshwater

In order to assess the adapted SEBS model, the model has been applied on two study areas under different atmospheric conditions and at different scales. ECMWF data and fieldwork data is used to validate the model over Victoria and Tana Lakes, respectively, as described in section 2.4.

5.1.4.1. Application SEBS over Lake Victoria (freshwater)

The adapted SEBS model was implemented over Lake Victoria to estimate the turbulent heat fluxes and the daily evaporation rate. (Table 5-4) shows a high agreement between the SEBS estimated sensible heat, latent heat, water heat flux as well as daily evaporation rate and ECMWF data. The RMSE of sensible heat, latent heat and water heat fluxes are 1.65 [W m^{-2}], 19.75 [W m^{-2}] and 19.85 [W m^{-2}], respectively. Thus, it can be shown that the overall uncertainty of the model output comes from the error in water heat flux estimation.

Table 5-4.a comparison between SEBS model and ECMWF model over Victoria Lake

in the period of (January 2010 - September 2012)

	water heat flux [W m^{-2}]		Sensible heat [W m^{-2}]		Latent heat [W m^{-2}]		daily evaporation [mm d^{-1}]	
	SEBS	ECMWF	SEBS	ECMWF	SEBS	ECMWF	SEBS	ECMWF
n	1005	1005	1005	1005	1005	1005	1005	1005
Average	110.2	110.9	3.9	4.2	51.4	51.0	4.8	4.8
STD	82.8	79.3	4.63	5.02	34.09	29.59	2.8	1.7
RMSE	19.9		1.7		19.8		1.5	
rRMSE (%)	6.7		4.1		8.9		7.4	

5.1.4.2. Application SEBS over Lake Tana (freshwater)

SEBS model has been applied over Lake Tana in the period between 06:00 p.m. 15th September 2011 and 06:00 p.m. 16th September 2011. Water heat flux was estimated using the water temperature profile method. The sum of the water heat flux during the day is -70 [W m^{-2}]. The negative value indicates that more energy transferred from the water to atmosphere than heat stored in the water body during the day. This excess energy was compensated by the heat energy transported through the water flow (Meehl, 1984).

The model results are compared with the Bowen model (Figure 5-23). (Table 5-5) shows a good agreement between the two models in the estimation of latent heat. It is found that SEBS model exhibits underestimation compared to Bowen model during the night time, when net radiation is negative, the gradient temperature is large and under high wind speed values. In the same regard, overestimation takes place under high net radiation values, and high gradient temperature and wind speed values. From this point of view, it can be shown that the net radiation is the most important parameter that should be estimated in an accurate way.

Table 5-5.a comparison between SEBS and Bowen model

	LE (SEBS)	LE (Bowen)	H (SEBS)	H (Penman constants)
n	23	23	23	23
Average	102.1	109.9	21.6	21.1
STD	226.3	193.8	13.7	17.2
MAD	29.2		3.5	
RMSE	35.6		4.8	

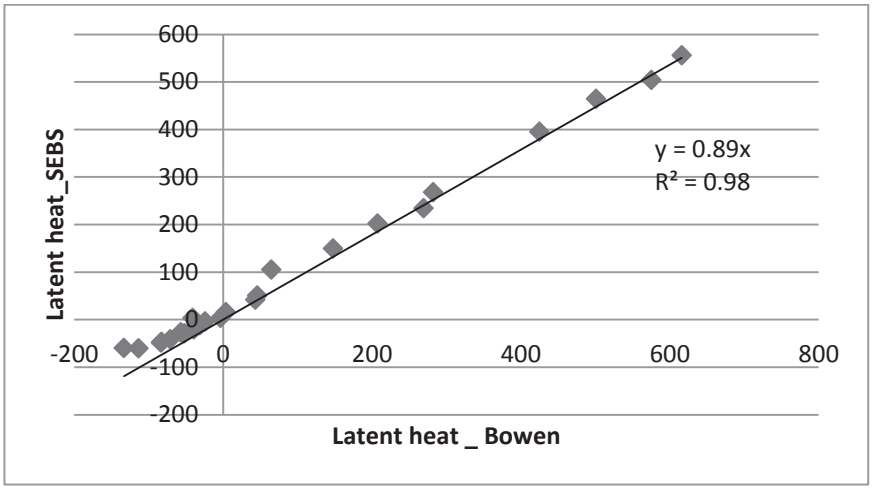

Figure 5-23.a comparison between latent heat of SEBS and Bowen models over Tana Lake

5.2. SEBS to saline water

5.2.1. Salinity Factor

The Salinity factor term was developed by (Turk, 1970). It is integrated into the adapted SEBS model to estimate the evaporation rate over saline water bodies. The salinity is in an inverse logarithmic relationship with the evaporation reduction value (Figure 5-24). The graph indicates that the influence of salinity upon the evaporation over fresh and brackish water 0 - 30 [g l^{-1}] is very limited (less than 1%). This influence increases gradually over saline and hypersaline water. When the salinity concentrations are 100 [g l^{-1}] and 300 [g l^{-1}], the reductions in evaporation are 3.4% and 31.9%, respectively.

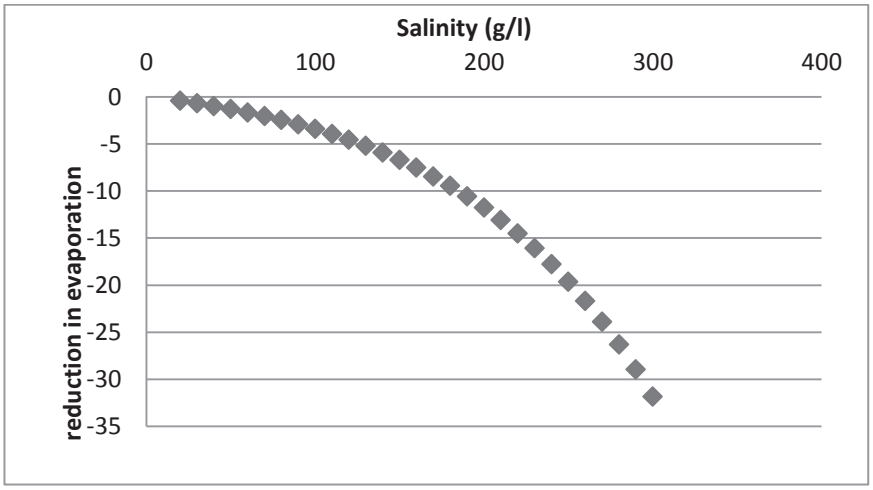

Figure 5-24.the relationship between salinity and reduction of evaporation

5.2.2. Application SEBS over Oceans

SEBS - salinity model has been applied over one degree of different oceans and seas to estimate the daily evaporation. The mean global salinity over Ocean is 34.7 [g l^{-1}] (Williams et al., 2010). It can be shown that the model follows ECMWF data in a good way (Table 5-6). The root mean square error (RMSE) of the estimated daily evaporation of the SEBS- Salinity model and original SEBS model over Indian Ocean are

0.21 and 0.25 [mm day^{-1}] respectively. This indicates that 1% reduction on the evaporation rate over oceans as a function of salinity. This is in an agreement approximately with (Kokya et al., 2008) observation which states that the evaporation rate over sea water reduces 0.94% due to the salinity effect.

The SEBS estimated heat fluxes have been validated with ECMWF data. Apparently, SEBS can estimate sensible heat flux in an accurate way (Table 5-7), where the deviation between the two models over different study areas is confined to 20 [W m^{-2}]. The efficiency of the SEBS sensible heat part is tested under different atmospheric parameters and stability. The wind speed ranges between 0.07- 20 [m s^{-1}], and the temperature gradient varies between (-4 and 8.5)^{0}k. High deviation takes place when the wind speed is higher than 10 [m s^{-1}] and the temperature gradient is larger than 4 ^{0}k. On the other hand, the highest underestimation occur under the same condition of wind speed and high negative value of the temperature gradient ranges between (-2 and 0) ^{0}k. This may be due to the inability of the stability equations to describe the real situation above the water surface under these conditions accurately.

Table 5-6.a comparison of daily evaporation between SEBS, SEBS-Salinity and ECMWF models

	Atlantic Ocean			Indian Ocean		
	original SEBS	SEBS salinity	ECMWF	original SEBS	SEBS salinity	ECMWF
n	1005	1005	1005	1005	1005	1005
Average [mm d^{-1}]	5.04	5.01	5.01	6.95	6.81	6.72
STD [mm d^{-1}]	1.88	1.86	1.85	2.70	2.68	2.63
RMSE [mm d^{-1}]	0.11	0.10		0.25	0.21	
rRMSE [%]	0.90	0.81		1.44	1.27	

Table 5-7.a comparison between Sensible heat of SEBS and ECMWF models

	Atlantic Ocean		Indian Ocean		Mediterranean Sea		Red Sea		North Sea	
	SEBS	ECMWF	SEBS	ECMWF	SEBS	ECMWF	SEBS	ECMWF	SEBS	ECMWF
n	1005	1005	1005	1005	1005	1005	974	974	1005	1005
Average [W m-2]	14.13	13.76	17.87	17.59	12.67	12.15	1.02	2.50	17.47	17.37
STD [W m-2]	9.70	9.52	11.52	11.63	21.77	23.02	13.99	12.85	27.98	31.00
RMSE [W m-2]	1.6		2.17		2.60		1.96		4.37	
rRMSE [%]	1.93		2.54		0.80		1.65		1.84	

The estimated latent heat follows the values of ECMWF data closely (Table 5-8). The error in the sensible and water heat fluxes estimation will reflect on the latent heat estimation. Therefore, the maximum average rRMSE is 14.3% over the North Sea, where the net shortwave and the dew temperature are low, the temperature gradient has low negative value, and the wind speed value is high; resulted in a high deviation in the water heat flux and sensible heat estimation.

Table 5-8.a comparison between latent heat of SEBS and ECMWF models

	Atlantic Ocean		Indian Ocean		Mediterranean Sea		Red Sea		North Sea	
	SEBS	ECMWF	SEBS	ECMWF	SEBS	ECMWF	SEBS	ECMWF	SEBS	ECMWF
n	1005	1005	1005	1005	1005	1005	974	974	1005	1005
Average [W m^{-2}]	151.1	145.1	181.7	194.6	120.9	120.5	100.8	128.6	101.1	57.1
STD [W m^{-2}]	55.9	56.7	79.7	78.5	103.8	77.7	63.0	68.7	94.3	54.1
RMSE [W m^{-2}]	26.9		33.7		51.1		37.6		77.5	
rRMSE [%]	6.8		7.0		8.6		10.5		14.3	

5.2.3. Application SEBS over the Great Salt Lake (Hypersaline Lake)

The SEBS salinity model has been applied over the Great Salt Lake. As the net shortwave radiation and the dew temperature are very low, a large deviation in the water heat flux estimation is obtained compare to ECMWF data. Since there is no vertical temperature profile available data, it is not possible to estimate the water heat flux using measured data. In order to achieve our objective and get a clear image about the influence of salinity upon evaporation rate over hypersaline-lake, ECMWF water heat flux is used to implement the adapted salinity - SEBS model upon this study area.

The results indicate a clear improvement in the instantaneous evaporation estimation by the SEBS-salinity model than the original SEBS model (Figure 5-25) with about 4% reduction in rRMSE and 0.25 [mm $3h^{-1}$] difference between the adapted and original models in terms of RMSE (Table 5-9). From this point of view; it can be concluded that the evaporation over Great Salt Lake is less by 26.5% approximately than the freshwater evaporation under the same atmospheric conditions.

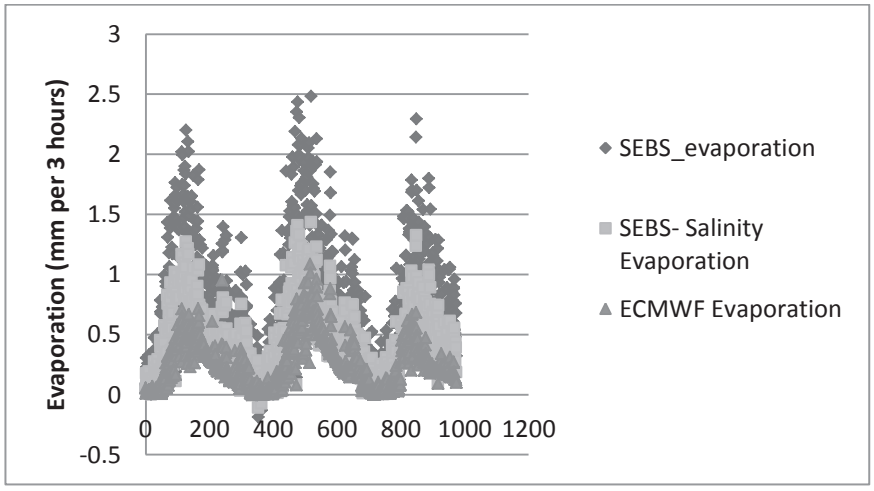

Figure 5-25.the instantaneous evaporation over Great Salt Lake

at 6:00 GMT using three different models in the period of January 2010 to September 2012

The sensible heat fluxes over saline water is larger than over freshwater. Thus, an underestimation of sensible heat is observed between SEBS and ECMWF results (Figure 5-26). The mean values of sensible

heat for the two models are 20.52 [W m^{-2}] and 94.42 [W m^{-2}], respectively, and the offset of the linear equation is 0.27. This is due to the conversion of the excess energy from the evaporation reduction process to other heat fluxes forms (Burba et al., 1999). In this regard, it can be concluded that the salinity reduces the proportion of the energy that is used for evaporation; therefore the excess energy converts to other heat fluxes forms. In oceans, most of this energy is converted to water heat flux form resulting in the increasing the convection layer (Meehl, 1984). On the other hand, in the inland shallow lake, most of this energy is converted to sensible heat form.

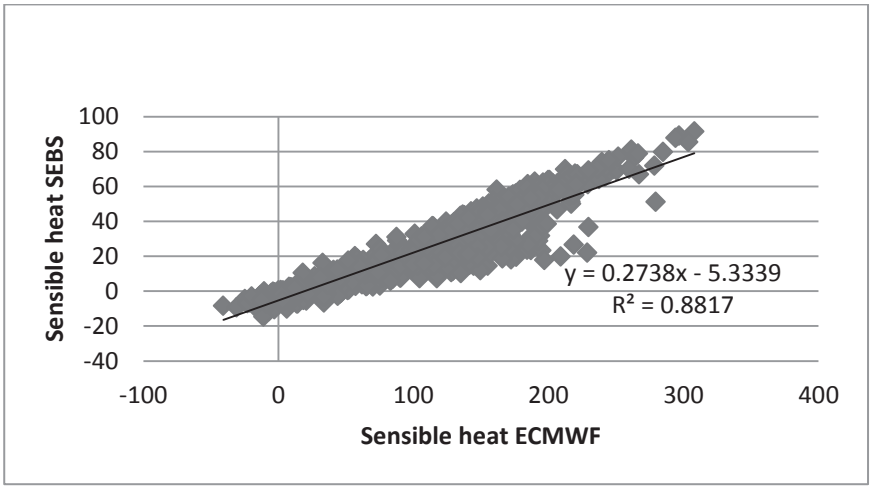

Figure 5-26.a comparison between the latent heat SEBS and ECMWF models over Great Salt Lake in the period of January 2010 to September 2012

Table 5-9.a comparison between different models of evaporation over Great Salt Lake in the period of January 2010 to September 2012

Statistical tools	SEBS	SEBS-Salinity	ECMWF
mean [mm $3h^{-1}$]	0.78	0.57	0.26
STD [mm $3h^{-1}$]	0.51	0.37	0.20
RMSE [mm $3h^{-1}$]	0.63	0.38	
rRMSE [%]	23.48	19.60	

5.2.4. Sensitivity of evaporation to salinity error measurement

The sensitivity of evaporation rate estimation to the error in the salinity measurements depends on the range of salinity concentration of the water body (Figure 5-27). If the salinity measurement overestimates by 10 [g l^{-1}] over its actual concentration 290 [g l^{-1}] and 20 [g l^{-1}], the error in the evaporation estimation will be about 2.65% and 0.23%, respectively. From this point of view, it can be concluded that the evaporation rate estimation is more sensitive to the error in the salinity measurement at higher level of salinity. This is due to the logarithmic relationship between the salinity concentration and its effect on the evaporation rate.

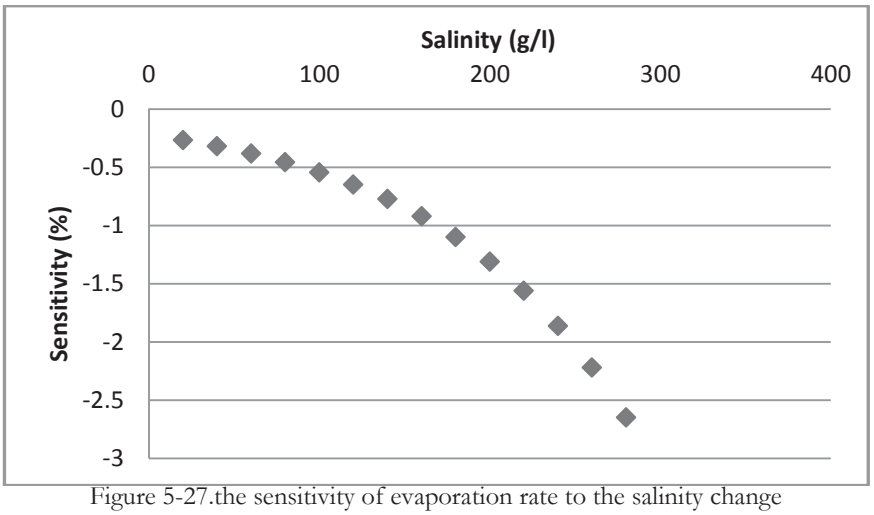

Figure 5-27.the sensitivity of evaporation rate to the salinity change respect to the previous salinity concentration

5.3. Application Adapted SEBS model using AATSR

The adapted SEBS model was implemented over different study areas using AATSR sea surface temperature images on January 2008 (Figure 5-28 and Figure 5-29). The ECMWF hydro-meteorological data resamples to 1 km using bi-cubic method.

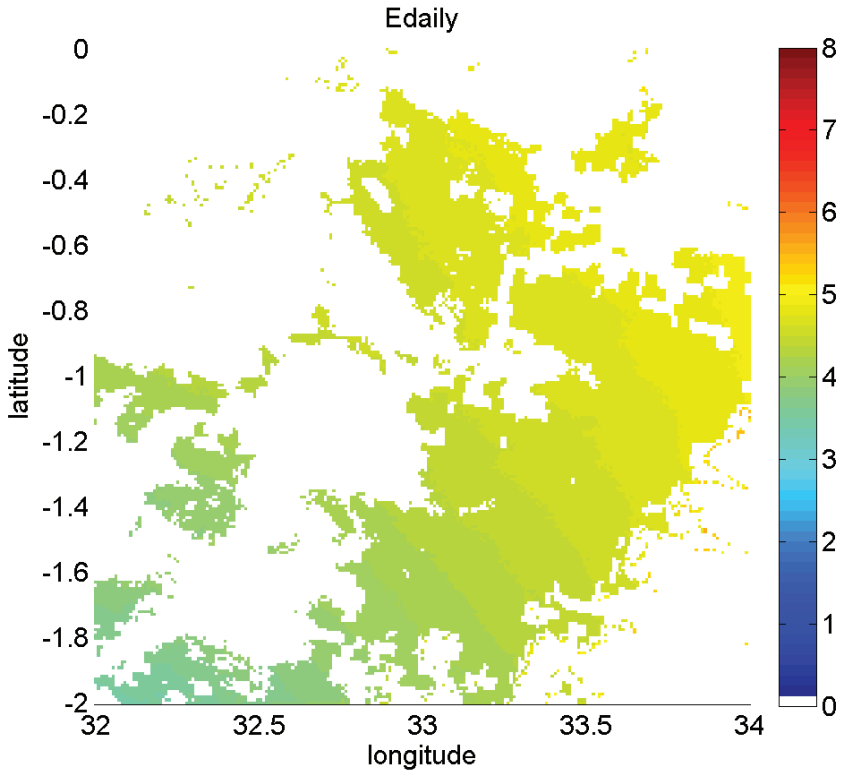

Figure 5-28.the daily evaporation over Victoria Lake on 10th January 2008 using AATSR

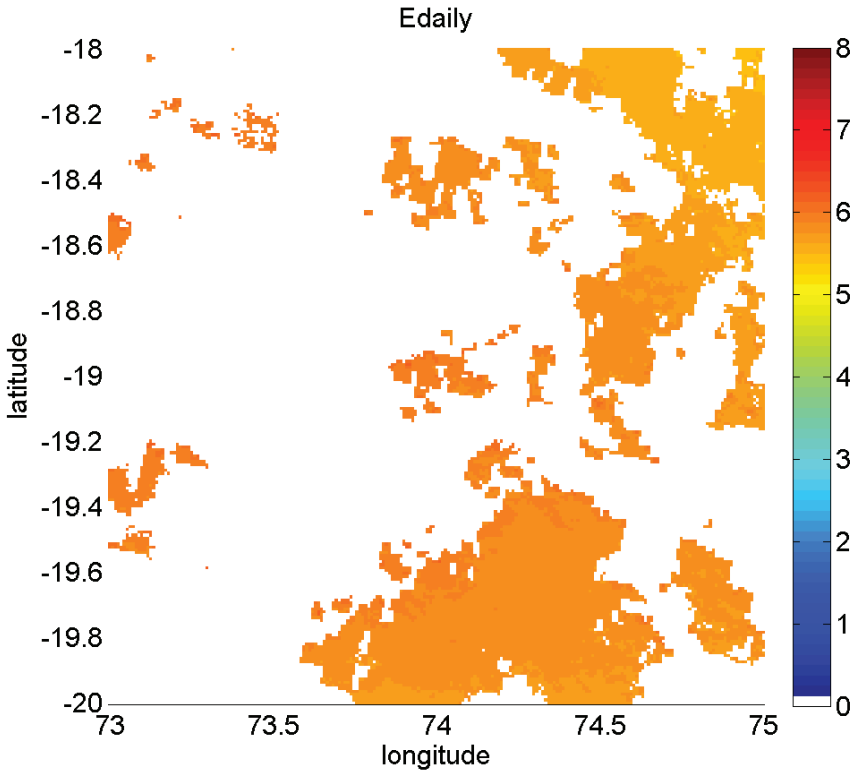

Figure 5-29.the daily evaporation over Indian Ocean on 3rd January 2008 using AATSR

6. CONCLUSION AND RECOMMENDATION

6.1. Conclusion

Various satellite models have been developed to estimate evaporation rates over water surfaces; however, most of them don't take the water composition parameters explicitly into account. One of the most important water quality parameters that affect the evaporation rate is the salinity concentration. Salinity affects the physical water characteristics such as water surface temperature and density; moreover, it reduces the vapour pressure on the water surface as well as it increases the amount of energy required to convert the water molecules from liquid to vapour state. Hence, the evaporation rate over saline water surfaces is less than over fresh water surfaces under the same atmospheric conditions. Therefore, the energy balance model has to take into account the salinity to estimate the evaporation rate accurately over fresh, saline and hypersaline water bodies.

SEBS is a remote sensing model which incorporates the physical state of the surface and the aerodynamic resistance in the calculation of the atmospheric turbulent fluxes, so it can be used to estimate the daily evaporation at a large scale. Unfortunately, this model has not been validated over water bodies. Therefore, this study aimed at adaption SEBS model to estimate the heat fluxes over fresh and saline water bodies. This main goal can be split up into the specific objectives:

a. Adapt the energy balance part of SEBS model to fresh water.
    1. Develop and validate a model to estimate the water heat flux.
    2. Estimate the roughness height of momentum and heat transfer.
    3. Validate the adapted SEBS model over fresh water bodies
b. Adapt the evaporation part of SEBS model to saline water.
    1. Estimate the sensitivity of the latent heat of vaporization to the salinity change.
    2. Analyses and estimate the influence of salinity upon evaporation of a large water body.
    3. Validate the adapted salinity – SEBS model over different water bodies with different salinities.

Firstly, the equilibrium thermal exchange method was incorporated to SEBS model to estimate the water heat flux parameter. This model exhibits a high agreement with ECMWF data with RMSE 26.8 [W m^{-2}] and rRMSE 4.3% over Atlantic Ocean. However, the model's efficiency decreases at low solar radiation and dew temperature values. The RMSE and rRMSE over the North Sea are 77.2 [W m^{-2}] and 8.5% respectively. Then, the eddy covariance data on Ijsselmeer Lake (the Netherlands) was used to estimate the aerodynamic resistance parameters. 90% of the total flux was contributed to the eddy covariance from a footprint area about 210 m. The roughness heights for momentum and heat transfer are 0.0002 m and

0.0001 m respectively. These parameters were validated on different study areas and under various atmospheric conditions. Eventually, In order to upscale the evaporation results from instantaneous to a daily basis, the available energy and evaporative fraction were investigated to be stable during the day. From this point of view, the evaporative fraction can be multiplied by the available energy at the overpass time of the satellite to estimate the daily latent heat and evaporation.

The adapted SEBS model was validated on Lake Victoria (Africa) and Lake Tana (Ethiopia). The heat fluxes results of the Victoria Lake are in the same order of magnitude as of the ECMWF data. The RMSE of the water heat flux, sensible heat flux and latent heat fluxes are 19.85 [W m^{-2}], 1.65 [W m^{-2}] and 19.75 [W m^{-2}], respectively. This indicates that the error in water heat flux estimation is mostly the main source of the overall error of the model. The mean daily evaporation on Lake Victoria is 1.75 [mm d^{-1}] with 0.01 [mm d^{-1}] underestimation than ECMWF. On the other hand, the estimated heat fluxes of Lake Tana are compared to the Bowen model results. The RMSE and rRMSE of the latent heat are 35.6 [W m^{-2}] and 4.75%, respectively. The model exhibits a high deviation than ECMWF and Bowen model under high wind speed and gradient temperature values. Hence, we can conclude that SEBS adapted model can be used to estimate the heat fluxes and the daily evaporation over fresh water bodies on different spatial scales in a good way.

The salinity factor was integrated with SEBS adapted model to estimate the evaporation rate over saline water bodies. The results show a clear improvement in evaporation estimation using SEBS-salinity model in comparison to the original SEBS model compare to ECMWF data as a reference over Great Salt Lake. RMSE of SEBS-salinity and original SEBS models over Great Salt Lake are 0.38 [mm $3h^{-1}$] and 0.63 [mm $3h^{-1}$] , respectively with 5% approximately improvement in terms of rRMSE when the salinity factor was integrated into SEBS to estimate the evaporation rate over saline water surfaces. On the other hand, a slight improvement takes place when the salinity integrated to SEBS to estimate the evaporation over oceans. RMSE of the SEBS-salinity and original SEBS models over Indian Ocean are 0.81 [mm d^{-1}] and 0.9 [mm d^{-1}], respectively. These results indicate that salinity reduces the evaporation rate over oceans and Great Salt Lake by 1% and 27%, respectively.

Finally, a sensitivity analysis was performed for assessing to which extent the uncertainty in the input parameters can contribute to the overall uncertainty of the model. It is illustrated that the order of sensitivity from the most to least influential input parameters to the estimated water heat flux are water surface temperature, dew temperature, wind speed, net solar radiation. Regarding to the sensible heat, it is shown that the gradient temperature is the main motivation force of it over water surfaces, as well as the sensitivity of sensible heat to the aerodynamic resistance is low. Lastly, it is proved that the error in the salinity measurement doesn't contribute to the uncertainty in the evaporation estimation largely under low salinity concentration conditions, but this sensitivity increases at high levels of salinity in a logarithmic way.

6.2. Recommendation

- Water surface temperature is the most sensitive parameter in this model, therefore, AATSR sea surface temperature with high accuracy 0.3° k and high spatial resolution 1 km should be the proper satellite image to apply this model.

- Equilibrium thermal exchange model is an appropriate method to estimate the water heat flux in a good way. It characterizes by few input parameters required; moreover, it reduces the limitation of field work measurements over water surfaces.

- It is proved that the ratio between water heat flux and net radiation is in a logarithmic relationship with the net radiation and net solar radiation. The parameters of this logarithmic equation change spatially and temporally. Defining the parameters affect the intercept and offset of the linear logarithmic equations should be a follow-up research to have a more accurate estimation of water heat flux to overcome the limitations of the equilibrium thermal exchange method.

- As it was mentioned in the first chapter, there are also some other water quality which can change the physical properties of the water and affect the energy balance terms; such as types of salts, phytoplankton and particulate matters concentration. Hence, studying the influence of these parameters on the evaporation process and the energy balance terms should follow up this research.

- Under high level of salinity concentration conditions, part of the available energy for evaporation process will convert to other forms of the heat fluxes. In inland lakes, this energy affects the aerodynamic resistance of the water surface and increases the sensible heat fluxes. Determining the roughness heights for momentum and heat transfer over hyper-saline lakes may improve the performance of the model on these lakes.

LIST OF REFERENCES

Abreham Kibret, A. (2009). *Open water evaporation estimation using ground measurements and satellite remote sensing : a case study of lake Tana, Ethiopia.* ITC, Enschede. Retrieved from http://www.itc.nl/library/papers_2009/msc/wrem/kibret.pdf (thesis)

Abualnaja, Y. (2009). Estimation of the Net Surface Heat Flux in the Arabian Gulf Based on the Equilibrium Temperature. *Journal of King Abdulaziz University, 20*(1), 21-29.

Ahmad F, & Sar, S. (1994). Equilibrium temperature as a parameter for estimating the net heat-flux at the air-sea interface in the central red-sea. *Oceanologica Acta, 17*(3), 341-343.

Al-Shammiri, M. (2002). Evaporation rate as a function of water salinity. *Desalination, 150*(2), 189-203. doi: 10.1016/s0011-9164(02)00943-8

Ali, H., Madramootoo, C. A., & Abdel-Dayem, S. (2000). Management of Lake Qaroun for salinity control. [Article]. *Icid Journal, 49*(1), 1-16.

Ali, H., Madramootoo, C. A., Abdel-Dayem, S., & Amer, M. H. (2000). Water and salt balance model of Lake Qaroun, Egypt. [Article]. *Icid Journal, 49*(3), 25-39.

Ali, H., Madramootoo, C. A., & Gwad, S. A. (2001). Evaporation model of Lake Qaroun as influenced by lake salinity. [Article]. *Irrigation and Drainage, 50*(1), 9-17. doi: 10.1002/ird.1

Belkin, I. M., Levitus, S., Antonov, J., & Malmberg, S.-A. (1998). "Great Salinity Anomalies" in the North Atlantic. *Progress In Oceanography, 41*(1), 1-68. doi: 10.1016/s0079-6611(98)00015-9

Brandt, R. E., Warren, S. G., Worby, A. P., & Grenfell, T. C. (2005). Surface albedo of the Antarctic sea ice zone. *Journal of Climate, 18*(17), 3606-3622. doi: 10.1175/jcli3489.1

Bromley, L. A., Singh, D., Ray, P., Sridhar, S., & Read, S. M. (1974). THERMODYNAMIC PROPERTIES OF SEA SALT-SOLUTIONS. *Aiche Journal, 20*(2), 326-335. doi: 10.1002/aic.690200218

Brutsaert, W. (1999). Aspects of bulk atmospheric boundary layer similarity under free-convective conditions. *Rev. Geophys., 37*(4), 439-451. doi: 10.1029/1999rg900013

Burba, G. G., Verma, S. B., & Kim, J. (1999). - Energy Fluxes of an Open Water Area in a mid-Latitude Prairie Wetland. *Boundary-Layer Meteorology, - 91*(- 3).

Cahill, A. T., Parlange, M. B., & Albertson, J. D. (1997). On the Brutsaert temperature roughness length model for sensible heat flux estimation. *Water Resources Research, 33*(10), 2315-2324. doi: 10.1029/97wr01638

Cragoa, R., & Brutsaert, W. (1996). Daytime evaporation and the self-preservation of the evaporative fraction and the Bowen ratio. *Journal of Hydrology, 178*(1–4), 241-255. doi: http://dx.doi.org/10.1016/0022-1694(95)02803-X

de Szoeke, S. P., Fairall, C. W., Wolfe, D. E., Bariteau, L., & Zuidema, P. (2010). Surface Flux Observations on the Southeastern Tropical Pacific Ocean and Attribution of SST Errors in Coupled Ocean-Atmosphere Models. *Journal of Climate, 23*(15), 4152-4174. doi: 10.1175/2010jcli3411.1

Diaz, X., Johnson, W. P., & Naftz, D. L. (2009). Selenium mass balance in the Great Salt Lake, Utah. *Science of The Total Environment, - 407*(- 7), - 2341.

Dickson, R. R., Meincke, J., Malmberg, S.-A., & Lee, A. J. (1988). The "great salinity anomaly" in the Northern North Atlantic 1968–1982. *Progress In Oceanography, 20*(2), 103-151. doi: 10.1016/0079-6611(88)90049-3

Edinger, J. E., Duttweiler, D. W., & Geyer, J. C. (1968). The Response of Water Temperatures to Meteorological Conditions. *WATER RESOURCES RESEARCH, - 4*(- 5), - 1143.

Finch, J. W. (2001). A comparison between measured and modelled open water evaporation from a reservoir in south-east England. [Article]. *Hydrological Processes, 15*(14), 2771-2778. doi: 10.1002/hyp.267

Font, J., Camps, A., Borges, A., Martin-Neira, M., Boutin, J., Reul, N., . . . Mecklenburg, S. (2010). SMOS: The Challenging Sea Surface Salinity Measurement From Space. [Article]. *Proceedings of the Ieee, 98*(5), 649-665. doi: 10.1109/jproc.2009.2033096

Haney, R., L. (1971). Surface Thermal Boundary Condition for Ocean Circulation Models. [Journal Article]. *Journal of Physical Oceanography, 1*(4), 7.

Harbeck, G. E. (1955). *The effect of salinity on evaporation*. Washington, DC: United States Gov. Print. Off.

Hudlow, M. D., Farnsworth, R. K., & Richards, F. P. (1983). EVAPORATION INTO THE ATMOSPHERE - THEORY, HISTORY, AND APPLICATIONS - BRUTSAERT,WH. [Book Review]. *Bulletin of the American Meteorological Society, 64*(5), 505-506.

Jia, L., Xi, G., Liu, S., Huang, C., Yan, Y., & Liu, G. (2009a). Regional estimation of daily to annual regional evapotranspiration with MODIS data in the Yellow River Delta wetland. *Hydrol. Earth Syst. Sci., 13*(10), 13.

Jia, L., Xi, G., Liu, S., Huang, C., Yan, Y., & Liu, G. (2009b). Regional estimation of daily to annual regional evapotranspiration with MODIS data in the Yellow River Delta wetland. *Hydrology and Earth System Sciences, 13*(10), 1775-1787.

Kaddumukasa, M., Nsubuga, D., & Muyodi, F. J. (2012). - Occurence of Culturable Vibrio cholerae from Lake Victoria, and Rift Valley Lakes Albert and George, Uganda. - *17*(- 4), - 299.

Kljun, N., Calanca, P., Rotachhi, M. W., & Schmid, H. P. (2004). A simple parameterisation for flux footprint predictions. *Boundary-Layer Meteorology, 112*(3), 503-523. doi: 10.1023/b:boun.0000030653.71031.96

Kokya, B. A., & Kokya, T. A. (2008). Proposing a formula for evaporation measurement from salt water resources. *Hydrological Processes, 22*(12), 2005-2012. doi: 10.1002/hyp.6785

Koloskov, G., Mukhamejanov, K., & Tanton, T. W. (2007). Monin-Obukhov length as a cornerstone of the SEBAL calculations of evapotranspiration. *Journal of Hydrology, 335*(1-2), 170-179. doi: 10.1016/j.jhydrol.2006.11.010

Le Vine, D. M., Lagerloef, G. S. E., & Torrusio, S. E. (2010). Aquarius and Remote Sensing of Sea Surface Salinity from Space. [Article]. *Proceedings of the Ieee, 98*(5), 688-703. doi: 10.1109/jproc.2010.2040550

Leaney, F. W. J. (2000). *Evaluating basin leakage rate, disposal capacity and plume development / Fred Leaney, Evan Christen*. Clayton, Vic. :: CRC for Catchment Hydrology.

Li, S., Kang, S., Li, F., Zhang, L., & Zhang, B. (2008). Vineyard evaporative fraction based on eddy covariance in an arid desert region of Northwest China. - *95*(- 8), - 948.

Liu, H. P., Peters, G., & Foken, T. (2001). New equations for sonic temperature variance and buoyancy heat flux with an omnidirectional sonic anemometer. *Boundary-Layer Meteorology, 100*(3), 459-468. doi: 10.1023/a:1019207031397

Liu, S., Lu, L., Mao, D., & Jia, L. (2007). Evaluating parameterizations of aerodynamic resistance to heat transfer using field measurements. *Hydrology and earth system sciences., 11*(2), 769-783.

Liu, S. M., Lu, L., Mao, D., & Jia, L. (2007). Evaluating parameterizations of aerodynamic resistance to heat transfer using field measurements. *Hydrology and Earth System Sciences, 11*(2), 769-783.

Llewellyn-Jones, D., & Remedios, J. (2012). The Advanced Along Track Scanning Radiometer (AATSR) and its predecessors ATSR-1 and ATSR-2: An introduction to the special issue. *Remote Sensing of Environment, 116*(0), 1-3. doi: 10.1016/j.rse.2011.06.002

Manrique Suñén, A. Beljaars, & I.Mammarella. (2012). *LAND SURFACE MODEL OVER FOREST AND LAKE SURFACES IN A BOREAL SITE- EVALUATION OF THE TILING METHOD*. Paper presented at the European Geosciences Union General Assembly EGU, Vienna, Austria. http://presentations.copernicus.org/EGU2012-2392_presentation.pdf

Marsh, P., & Bigras, S. C. (1988). EVAPORATION FROM MACKENZIE DELTA LAKES, NWT, CANADA. [Article]. *Arctic and Alpine Research, 20*(2), 220-229. doi: 10.2307/1551500

Meehl, G. A. (1984). Calculation of ocean heat storage and effective ocean surface layer depths for the northern hemisphere. *Journal Name: J. Phys. Oceanogr.; (United States); Journal Volume: 14:11*, Medium: X; Size: Pages: 1747-1816.

Mengistu, M. G., & Savage, M. J. (2010). Open water evaporation estimation for a small shallow reservoir in winter using surface renewal. *Journal of Hydrology, 380*(1–2), 27-35. doi: 10.1016/j.jhydrol.2009.10.014

Murray, T., & Verhoef, A. (2007). Moving towards a more mechanistic approach in the determination of soil heat flux from remote measurements - II. Diurnal shape of soil heat flux. [Article]. *Agricultural and Forest Meteorology, 147*(1-2), 88-97. doi: 10.1016/j.agrformet.2007.06.009

Nauš, J. (1999). Campbell, G.S., Norman, J.M.: An Introduction to Environmental Biophysics. *Photosynthetica, 36*(1), 30-30. doi: 10.1023/a:1007016114990

Nichols, W. E., & Cuenca, R. H. (1993). Evaluation of the evaporative fraction for parameterization of the surface energy balance. *Water Resources Research, 29*(11), 3681-3690. doi: 10.1029/93wr01958

Nuru A, Molla B, & E, Y. (2012). Occurrence and distribution of bacterial pathogens of fish in the southern gulf of Lake Tana, Bahir Dar, Ethiopia. *Livestock Research for Rural Development, 24*(149).

Oroud, I. M. (1999). Temperature and evaporation dynamics of saline solutions. *Journal of Hydrology, 226*(1–2), 1-10. doi: 10.1016/s0022-1694(99)00138-9

Owen, P. R., & Thomson, W. R. (1963). HEAT TRANSFER ACROSS ROUGH SURFACES. *Journal of Fluid Mechanics, 15*(3), 321-334. doi: 10.1017/s0022112063000288

Papale, D., Reichstein, M., Aubinet, M., Canfora, E., Bernhofer, C., Kutsch, W., . . . Yakir, D. (2006). Towards a standardized processing of Net Ecosystem Exchange measured with eddy covariance technique: algorithms and uncertainty estimation. *Biogeosciences, 3*(4), 571-583.

Rwasoka, D. T., Reyes-Acosta, J. L., van der Tol, C., Su, Z., & Lubczynski, M. W. (2010). Evapotranspiration in water limited environments : up - scaling from the crown canopy to the eddy flux footprint + poster. *In: Geophysical Research Abstracts, 12(2010) EGU2010-15540, EGU general assembly 2010. 1 p.*

Salhotra, A. M., Adams, E. E., & Harleman, D. R. F. (1987). The alpha, beta, gamma of evaporation from saline water bodies. *Water Resources Research, 23*(9), 1769-1774. doi: 10.1029/WR023i009p01769

Schmid, H. P. (1997). Experimental design for flux measurements: matching scales of observations and fluxes. *Agricultural and Forest Meteorology, 87*(2-3), 179-200. doi: 10.1016/s0168-1923(97)00011-7

Schmitt, V., & Lequeux, F. (1995). S.A.N.S. Spectra and Elastic Plateau Modulus in a Charged Wormlike Micelles Solution: Effect of Salt. *J. Phys. II France, 5*(2), 193-197.

Schotanus, P., Nieuwstadt, F. T. M., & Bruin, H. A. R. (1983). Temperature measurement with a sonic anemometer and its application to heat and moisture fluxes. *Boundary-Layer Meteorology, 26*(1), 81-93. doi: 10.1007/bf00164332

Schuepp, P. H., Leclerc, M. Y., Macpherson, J. I., & Desjardins, R. L. (1990). FOOTPRINT PREDICTION OF SCALAR FLUXES FROM ANALYTICAL SOLUTIONS OF THE DIFFUSION EQUATION. *Boundary-Layer Meteorology, 50*(1-4), 353-373.

Sharqawy, M. H., Lienhard, J. H., & Zubair, S. M. (2011). Thermophysical properties of seawater: A review of existing correlations and data (vol 16, pg 354, 2010). *Desalination and Water Treatment, 29*(1-3), 355-355. doi: 10.5004/dwt.2011.2947

Shuttleworth, W. J., Gurney, R. J., Hsu, A. Y., & Ormsby, J. P. (1989). *FIFE: The variation in energy partition at surface flux sites*.

Sollie, S., Coops, H., & Verhoeven, J. T. A. (2008). Natural and constructed littoral zones as nutrient traps in eutrophicated shallow lakes. [Article]. *Hydrobiologia, 605*, 219-233. doi: 10.1007/s10750-008-9356-6

Stewart, J. B., & Thom, A. S. (1973). ENERGY BUDGETS IN PINE FOREST. *Quarterly Journal of the Royal Meteorological Society, 99*(419), 154-170. doi: 10.1002/qj.49709941913

Su, Z. (2002a). The Surface Energy Balance System (SEBS) for estimation of turbulent heat fluxes. [Article]. *Hydrology and Earth System Sciences, 6*(1), 85-99.

Su, Z. (2002b). surface energy balance system SEBS for estimation of turbulent heat fluxes. *JournalHydrology and earth system sciences (HESS) : open access, 6*(1), 85-99.

Su, Z., Schmugge, T., Kustas, W. P., & Massman, W. J. (2001). evaluation of two models for estimation of the roughness height for heat transfer between the land surface and the atmosphere. *In: Journal of applied meteorology, 40(2001)11, pp. 1933-1951.*

Tanny, J., Cohen, S., Assouline, S., Lange, F., Grava, A., Berger, D., . . . Parlange, M. B. (2008). Evaporation from a small water reservoir: Direct measurements and estimates. *Journal of Hydrology, 351*(1-2), 218-229. doi: 10.1016/j.jhydrol.2007.12.012

Thom, A. S. (1972). MOMENTUM, MASS AND HEAT-EXCHANGE OF VEGETATION. *Quarterly Journal of the Royal Meteorological Society, 98*(415), 124-&. doi: 10.1002/qj.49709841510

Tian, X., Li, Z. Y., van der Tol, C., Su, Z., Li, X., He, Q. S., . . . Li, L. H. (2011). Estimating zero-plane displacement height and aerodynamic roughness length using synthesis of LiDAR and SPOT-5 data. *Remote Sensing of Environment, 115*(9), 2330-2341. doi: 10.1016/j.rse.2011.04.033

Turk, L. J. (1970). Evaporation of Brine: A Field Study on the Bonneville Salt Flats, Utah. *Water Resources Research, 6*(4), 1209-1215. doi: 10.1029/WR006i004p01209

van der Tol, C., & Parodi, G. N. (2012). Guidelines for remote sensing of evapotranspiration. *In: Evapotranspiration : remote sensing and modeling / ed. by A. Irmak. - Rijeka : InTech, 2012. 514 p ISBN 978-953-307-808-3 pp. 227-250.*

Vesala, T., Kljun, N., Rannik, U., Rinne, J., Sogachev, A., Markkanen, T., . . . Leclerc, M. Y. (2008). Flux and concentration footprint modelling: State of the art. *Environmental Pollution, 152*(3), 653-666. doi: 10.1016/j.envpol.2007.06.070

Williams, P. D., Guilyardi, E., Madec, G., Gualdi, S., & Scoccimarro, E. (2010). The role of mean ocean salinity in climate. *Dynamics of Atmospheres and Oceans, 49*(2–3), 108-123. doi: 10.1016/j.dynatmoce.2009.02.001

Winter, T. C., Rosenberry, D. O., & Sturrock, A. M. (1995). EVALUATION OF 11 EQUATIONS FOR DETERMINING EVAPORATION FOR A SMALL LAKE IN THE NORTH CENTRAL UNITED-STATES. [Article]. *Water Resources Research, 31*(4), 983-993. doi: 10.1029/94wr02537

Wurtsbaugh, W. A., Gardberg, J., & Izdepski, C. (2011). Biostrome communities and mercury and selenium bioaccumulation in the Great Salt Lake (Utah, USA). *Science of The Total Environment, - 409*(- 20), - 4434.

Zhou, Y. L., Ju, W. M., Sun, X. M., Wen, X. F., & Guan, D. X. (2012). Significant Decrease of Uncertainties in Sensible Heat flux Simulation Using Temporally Variable Aerodynamic Roughness in Two Typical Forest Ecosystems of China. [Article]. *Journal of Applied Meteorology and Climatology, 51*(6), 1099-1110. doi: 10.1175/jamc-d-11-0243.1

APPENDIX

Appendix 1: SEBS model

Energy balance equation

$$R_n = G_0 - H - \lambda E$$

Net radiation

$$R_n = R_s \downarrow - R_s \uparrow + R_L \downarrow - R_L \uparrow$$

$$R_n = (1 - \alpha) R_s \downarrow + \varepsilon_a \sigma {T_a}^4 - \varepsilon_0 \sigma {T_0}^4$$

R_s	:	Incoming shortwave radiation	[W m^{-2}]
T_a	:	Temperature of the air at the reference height	[k]
T_0	:	Temperature of the water surface	[k]
ε_0	:	Emissivity of the water surface	[-]
ε_a	:	Emissivity of the air	[-]
α	:	Surface albedo	[-]
σ	:	Boltzman constant = 5.678 x 10^{-8}	[Wm^{-2}k^4]

The albedo of the water surface will be taken as a constant value α = 0.07 (Brandt et al., 2005) and the emissivity is 0.99 (Abreham Kibret, 2009)
the air emissivity is estimated from the temperature of the air [°c] using (Nauš, 1999)Model :

$$\varepsilon_a = 9.2*10^{-6} \left(T_a\text{-}273.15\right)^2$$

Sensible heat

$$u = \frac{u^*}{k}\left[\ln\left(\frac{z - d_0}{z_{0m}}\right) - \varphi_m\left(\frac{z-d_0}{z_{0m}}\right) + \varphi_m\left(\frac{z_{0m}}{L}\right)\right]$$

$$(\theta_0 - \theta_a) = \frac{H}{K\, u^* \rho C_p}\left[\left(\ln\left(\frac{Z-d_0}{Z_{0h}}\right) - \varphi_h\left(\frac{z-d_0}{L}\right) + \varphi_h\left(\frac{z_{oh}}{L}\right)\right)\right]$$

$$L = \frac{\rho\, c_p\, {u^*}^3 \theta_v}{K\, g\, H}$$

Z_{0m}	:	surface roughness length for momentum transfer	[m]
d_0	:	zero plane displacement	[m]
H	:	sensible heat flux [Wm^{-2}]	
Z	:	reference height above the water surface	[m]
L	:	Monin-Obukhov length	[m]
ρ_a	:	air density	[kgm^{-3}]
C_p	:	specific heat of air at constant pressure	[J kg^{-1}k^{-1}]
u^*	:	friction velocity	[ms^{-1}]
k	:	Von Karman's constant = 0.4	[-]
B	:	Stanton number	[-]

u	:	velocity of air	[ms^{-1}]
θ_0	:	potential temperature of the water surface	[k]
θ_a	:	potential temperature of air at reference height Z	[k]

They can be calculated as

$$\theta_{0,a} = T_{0,a}\left(\frac{P_0}{P_{ref}}\right)^{0.286}$$

P_0	:	pressure at the water surface	[hPa]
P_{ref}	:	pressure at reference height	[hPa]
L	:	Monin-Obukhov length	[m]
g	:	gravitational acceleration = 9.80665	[ms^2]
θ_v	:	virtual temperature (k). It can be defined as:	

$$\theta_v = \theta_a(1+0.61\mathrm{Q})$$

Q	:	maximum Humidity Ratio	[kg kg^{-1}]
φ_m	:	stability correction functions formomentum transfer	
φ_h	:	stability correction function for heat transfer	

Latent heat

Latent energy λE can be defined as:

$$\lambda E = EF\ (R_n - G_0)$$

The evaporative fraction is the ratio between actual evaporation and the available amount of energy. It can be estimated using the following equation:

$$EF = \lambda E_{wet}\left(\frac{EF_r}{(R_n - G_0)}\right)$$

The limitation of the sensible heat flux can be used mathematically to estimate the relative evaporative fraction value.

$$EF_r = \frac{\lambda E}{\lambda E_{wet}} = 1 - \frac{\lambda E_{wet} - \lambda E}{\lambda E_{wet}} = 1 - \frac{H - H_{wet}}{H_{dry} - H_{wet}}$$

$$H_{dry} = R_n - G_0$$

$$H_{wet} = R_n - G_0 - \lambda E_{wet}$$

Mathematically, it can be calculated using the following formula:

$$H_{wet} = \frac{\left[(R_n - G_0) - \frac{\rho\, c_p}{r_{ew}} \cdot \frac{e_s - e_a}{\gamma}\right]}{\left(1 + \frac{\Delta}{\gamma}\right)}$$

Where

γ	:	psychometric constant	[hPa °c^{-1}]
Δ	:	rate of change of saturation vapour pressure with temperature	[hPa °c^{-1}]
e_s	:	water vapour pressure in. It can parameterize as:	[hpa]

$$e_s = 6.107 \cdot 10^{\frac{7.5 \cdot T}{237.3 + T}}$$

e_a :actual water vapor pressure [hpa]

It can be defined as:

$$e_a = 611 * 10^{7.5\left(\frac{T_a - 273.15}{T_a - 35.86}\right)}$$

r_{ew} :external resistance at the wet limit.

r_{ew}value depends on the Monin-Obukhov length which is parameterized using the wind friction and the sensible heat flux variables.

$$\mathrm{r_{ew}} = \frac{1}{\mathrm{ku^*}}\left(\ln\left(\frac{\mathrm{Z\text{-}d_0}}{\mathrm{z_{0h}}}\right) - \varphi_\mathrm{h}\left(\frac{\mathrm{z\text{-}d_0}}{\mathrm{L_w}}\right) + \varphi_\mathrm{h}\left(\frac{\mathrm{z_{oh}}}{\mathrm{L_w}}\right)\right)$$

The Monin-Obukhov length at wet limit can be defined as:

$$\mathrm{L_w} = \frac{\rho\, \mathrm{u^{*3}}}{\mathrm{K\, g\, 0.61\, (\frac{Rn\text{-}G^0}{\lambda})}}$$

$\lambda E_{wet}$is the latent heat at wet limit. It is determined using penman equation as following:

$$\lambda E_{wet} = R_n - G_o - H_{wet}$$

Daily evaporation

$$\lambda \mathrm{E_{daily}} = 86400 * 10^3 * \mathrm{EF}\,(\mathrm{R_n} - \mathrm{G_0})$$

The latent heat is converted to water depth in (mm) per unit of time

Then the daily evaporation can be calculated as a water depth by using the following equation:

$$E_{daily} = \frac{\lambda \mathrm{E_{daily}}}{\lambda\, \rho_\mathrm{w}}$$

E_{daily} :	daily evaporation		[mm day^{-1}]
ρ_w :	water density		[kg m^{-3}]